공학석사학위논문

Core-Shell Structured Carbonyl Iron With Polystyrene Foam Microparticles Designed for Enhanced Sedimentation Stability and Its Magnetorheology

향상된 침전 특성을 갖는 폴리스티렌 미세 발포 입자로 코팅된 코어-쉘 구조의 마이크로 카르보닐 철의 제조와 자기유동학적 특성

2015년 2월

서울대학교 대학원

재료공학부

좌웨이환

Core-Shell Structured Carbonyl Iron With Polystyrene Foam Microparticles Designed for Enhanced Sedimentation Stability and Its Magnetorheology

지도교수 서용석

이 논문을 공학 석사 학위논문으로 제출함

2015년 2월

서울대학교 대학원

재료공학부

좌웨이환

좌웨이환의 공학 석사 학위논문을 인준함

2014년 12월

위 원 장 _____ (인)

부위원장 _____ (인)

위 원 _____ (인)

ABSTRACT

Core-Shell Structured Carbonyl Iron With Polystyrene Foam Microparticles Designed for Enhanced Sedimentation Stability and Its Magnetorheology

Chuah Wei Huan
Materials Science and Engineering
The Graduate School
Seoul National University

The sedimentation stability of carbonyl iron (CI)-based magnetorheological (MR) fluids was enhanced by applying a dual-step processing comprising coating a PS layer on the CI particles surfaces via conventional dispersion polymerization, subsequently by the foaming of the PS coating layer using the supercritical carbon dioxide fluid foaming processing to produce a core-shell structured CI coated with Polystyrene foam (CI/PSF) particle. The reduction of density after coating and foaming modification was verified using a pycnometer and the surface morphologies

were observed by SEM. The specific surface areas were determined by Brunauer–Emmett–Teller (BET) adsorption measurements to study the change in surface roughness upon modification. The elemental analysis was done to confirm the foaming processing did not contaminate the product. The influence of the volume expansion after modification on the magnetic properties was investigated by analyzing the MR performance using a vibrating sample magnetometer and rotational rheometer. Finally, the sedimentation properties of the synthesized particles was examined using Turbiscan apparatus. MR fluids containing the newly developed CI coated with Polystyrene foam (CI/PSF) particles exhibited remarkable stability against sedimentation essentially attributed to the reduced mismatch in density between particles and the carrier medium.

Keywords : Magnetorheological fluid, Carbonyl Iron, Polystyrene foam, Core-Shell structure, Supercritical Carbon Dioxide fluid.

Student Number : 2013-22470

CONTENTS

CHAPTER 3. RESULTS AND DISCUSSION

LIST OF FIGURES

LIST OF TABLES

CHAPTER 1. INTRODUCTION

1.1 Magnetorheological (MR) Fluids

The use of external fields to control the microstructure of colloidal suspensions has long been recognized as a powerful means for tailoring the mechanical, optical and electronic properties of materials. Magnetorheological (MR) suspensions, in particular, provide a striking example. These normally stable fluids undergo a dynamic transition to a solid with milliseconds upon the application of an external magnetic field. Therefore, considerable effort has gone into research of MR fluids to understand the fundamental science around this field responsive fluids in the hopes of better defining the particle dynamics of MR fluids to help understand adaptable the fluids for use in industrial applications. One such project is the NASA's Investigating the Structure of Paramagnetic Aggregates from Colloidal Emulsions (InSPACE) experiments that have been performed on the International Space Station to explore the structural transition of MR fluids in microgravity where gravity is essentially absent. New discovery resulting from InSPACE studies could be used to improve or develop active mechanical systems in engineering implementation.[1]

Typical MR fluids are formulated by dispersion of micron-sized

ferromagnetic or ferromagnetic particulates in a carrier liquid, usually a mineral or synthetic oil depending on the desired properties. The carrier fluid serves as a dispersed medium and ensures the homogeneity of particles in the fluid. By application and removal of an externally applied magnetic field, MR fluids have the unique ability to rapidly and reversibly transform from a fluid-like to a solid-like state in a matter of milliseconds, showing instantaneous and tunable changes of several orders of magnitudes in rheological properties. Without an external magnetic field, in terms of their consistency, MR fluids behave similar to those of the carrier fluid as a viscous liquid and the magnetic particles are randomly dispersed in the carrier liquid medium. Conversely, the apparent viscosity of MR fluids increases significantly when subjected to a magnetic field and becomes a viscoelastic solid. When an external magnetic field is imposed, the magnetic particles attract one another and build up chain-like structures aligned in the field direction due to an induced magnetic dipole-dipole interaction between neighboring particles. Spanning the gap of a flowing channel, these chain-like structures hinder the flow of the carrier fluid thereby increase the viscosity characteristics of MR fluids.[2] The rheological behavior of MR fluids with the presence of a magnetic field is typically described by the Bingham plastic model. A material with a yield stress in a magnetic field does not flow unless the shear stress applied exceeds the yield

stress.[3] In other words, the rheological properties (including yield stress, apparent viscosity, and storage modulus) of MR fluids can vary incredibly with the magnetic field intensity, enabling fine-tuning of the material behavior.

1.2 Applications of MR fluids

This salient field-responsive property inherently appropriate for applications in mechanical systems that require the active control of vibrations or the transmission of torque. A representative application area is the automotive industry where the variable nature of MR fluids has been put to use in semi-active smart vibration-absorption systems[4], primary vehicle suspension systems, adaptive crew seats for vibration[5], clutches, power steering pumps, torque transducer and so on.[6] Especially noteworthy is the development of the so-called MR fluid based active suspension system known as MagneRide^{TM}, developed by Delphi Automotive Systems.[7] It uses an entirely new form of damping technology that resolves the age-old conflict between comfort and driving dynamics/safety without countenancing any of the otherwise unavoidable compromises. The damping force is only dependent on the electromagnetic field intensity applied to the MR fluid. The magnetic field changes the state of the fluid to deliver variable damping. Since no mechanical parts must be moved, the MR damper responds extremely

spontaneously. As a continuously adaptive system, it adapts the damping characteristic to the profile of the road and can be adjusted in a matter of milliseconds. So, it provides the right degree of damping force at each individual wheel in every situation. Ever more powerful engines and faster cars mean that suspension systems have become a vital development aspect in the automotive industry.[8] And this active suspension system will play an increasingly important role in the future, because the chassis ─ particularly the springs and shock absorbers ─ provides the connection between the wheel suspension and the car body, ensuring optimum contact with the road. A simplified explanation for the active suspension system could prove beneficial in improving driving safety is as follows. The greater damping force results in steadier and tighter handling along with better control in the threshold. Also, it optimally suppresses the rolling tendency of the vehicle's body in corners. On a larger scale, MR suspension system can be found in China's Dong Ting Lake Bridge to counteract vibrations caused by sudden gusts of wind.[9] The same principle is also being applied to stabilize buildings against earthquakes. When sensors on the buildings sense disturbance, they send signals to supply an electrical charge to the dampers.[10] The MR fluid in these dampers changes state constantly in line with the movement of the building, acting as a huge shock absorber. Other examples involves the use of MR finishing for the

commercial manufacture of high precision optics. MR finishing is a magnetic field-assisted precision finishing process that utilizes MR polishing fluid to polish different kinds of materials. The MR polishing fluid, consists of magnetic particles and non-magnetic abrasive particles dispersed in a carrier liquid, forms a conformal polishing tool and therefore it can polish a variety of shapes, including flat, convex, and concave, to sub-nanometer surface roughness value.[11]

1.3 Sedimentation Problems and Solutions Proposed

MR fluids and devices have made substantial progress towards commercialization. Nonetheless, several problems exist, the challenges in this area are still daunting, but appear surmountable. For instance, the sedimentation of magnetic particles within the MR suspension due to the critical mismatch/imbalance between the high density of the magnetic substances and the relatively low density of the carrier liquid, the poor re-dispersibility of settled particles after caking, or the weak chemical degradation resistance of magnetic particles, all of which can limit MR fluids to be further utilized in industrial applications.[12] In order to overcome these crucial restriction factors, various methods, including polymer coating techniques[13]; passivation layers on magnetic particles formation[14]; the use of

viscoplastic medium as a carrier liquid; adding different types of additives[15], fillers or surfactants; and the use of non-spherical particles-based[16] or bidispersed MR suspensions[17], have been widely introduced. The use of suspension containing strictly nanoparticles can remain suspended in the fluid indefinitely due to Brownian motion by thermal convection. Addition of nanoparticles to the suspension effectively mitigates sedimentation however, increasing the nanoparticles concentration causes the apparent yield stress of the MR fluids to decay by several order of magnitudes. Moreover, recent studies by Sutrisno *et al* has advocated that the settling rate of a bidispersed MR fluid composed of light polymeric non-magnetic microspheres (particle size range from 55 to 85 μm and density of 0.03 g cm^{-3}) dispersed in the conventional MR fluid was reduced and it demonstrated improved redispersion because the large microparticles fill pores which are created between the magnetic particles.[18] Few studies have clarified the influence of shape on the suspension stability which stability can be improved by replacing spherical iron particles with the plate-like iron particles so as to eliminate the sedimentation velocity.[16] Bell *et al* have proposed that Iron nanofiber based MR fluids have exhibited promising results for not only reducing or preventing sedimentation, but also display increased yield stress of the nanofiber based suspension.[19] The difference in the sedimentation between

nanofiber and sphere based suspensions is a result of nanofiber entanglement that occurs in concentrated suspensions of long slender particles as the motion of fibers is severely restricted. Furthermore, many factors must be considered to understand the increase in the apparent yield stress of the nanofiber based fluids as compared to the sphere based fluids. The difference in the size of the fibers compared to spherical particles caused a direct comparison between the properties of the two types of suspensions difficult to interpret, to form conclusions, or to infer the underlying physics. Besides, another most frequently used methods to stabilize heavy magnetic particles in MR suspensions consists in adding thickening agents (usually high molecular weight polymers) that hinder the particle settling because of high viscosity that they impart to the carrier liquid.[15] But this type of system suffers from the trade-off between increasing suspension stability and diminishing in possible range of controllable viscosities. Ideal MR fluids have low viscosities giving them the largest possible range of controllable viscosities and allowing for easy flow within a device. Among approaches proposed above, the coating of magnetic particles with an appropriate surface layer seems to be one of the most efficient variants since it not only improves sedimentation stability by decreasing particles density, and enhances durability and chemical resistance but also positively affects the surface free energy of magnetic particles which

consequently results in superior mutual compatibility ─ higher wettability ─ with the carrier liquid.[20]

In the development of novel MR suspensions with enhanced sedimentation stability feature, attention is nowadays predominantly focused on applying polymer/inorganic substance coatings to magnetic particle surfaces forms the familiar core-shell structure particles and decreases the density of magnetic metal/polymer composite particles. Carbonyl Iron (CI), which is a type of highly pure iron made by the chemical vapor deposition decomposition of iron pentacarbonyl, appears to be the main workhorse of most practical MR fluid compositions because of their excellent MR characteristics with their less magnetic hysteresis and high saturation magnetization value, as well as proper particle size in the range of 1~10 μm.[21] Accordingly, the large density of CI particles (density of approximately 7.8 g cm^{-3}), which causes a serious sedimentation problem, has gained a great deal of interest from both academia and industry to resolve that problem. To solve the sedimentation problems associated with Carbonyl Iron (CI)-based MR suspensions, dual-step functionality coatings has been even adopted to deposit a polymer shell and a multiwalled carbon nanotubes nest on the CI particle surfaces, rather than using a single polymer or multiwalled carbon nanotubes layer coating. The density was reduced from 7.91 g cm^{-3} for pure CI particles to 6.88 g cm^{-3} for

CI/Polymer particles and 6.7 g cm^{-3} for CI/Polymer/Multiwalled carbon nanotubes particles.[22] Note that sequential coating with polymer and multiwalled carbon nanotubes has also been reported.[23] Beyond these classical solutions, effective strategies to reduce the density of polymer coating particles have been, according to our best knowledge, studied only rarely. As a result, in the present study, a genuinely new core-shell structured CI coated with Polystyrene (PS) foam microparticles has been fabricated for the purpose of sedimentation stability enhancement. However, the processing method to make this kind of polymer foam microparticles has not yet been fully defined. Particularly noteworthy is the synthesis of polymer foam microparticles using supercritical carbon dioxide ($scCO_2$) foaming technology.

1.4 Supercritical Carbon Dioxide ($scCO_2$) Foaming

The most common polymer foams are polystyrene foam (Styrofoam) and polyurethane foam. A polymer foam is polymer-and-gas mixture, comprising gas bubbles entrapped in a continuous polymer matrix phase, which gives the material a porous or cellular structure. The characteristic properties of a foamed polymer include low density, high strength per unit weight, good thermal insulation, and good energy absorbing qualities. Hence, these outstanding features, in particular light weight, of the polymer foam make it

ideally suited for implementation in creating low density CI encapsulated with polymer foam composite particles.

Foam generation with $scCO_2$ has recently been a popular topic of research because of its non-toxic and environmentally benign produce stems from the fact that $scCO_2$ fluid may replace many environmentally harmful, volatile organic solvents currently used in industry.[24] The advantage of $scCO_2$ over conventional foaming technique with liquid solvents is that the fluid penetrates the polymer material efficiently and can be removed from the foamed polymeric product, without leaving a trace, simply by lowering the pressure below the critical value. Porous polymeric foam products can be easily obtained without additional post-treatment, thereby avoiding costly solvent-removing processes.[25,26]

A supercritical fluid is defined as a substance above its critical pressure and temperature. A typical pressure-temperature phase diagram is shown in Figure 1. Carbon dioxide (CO_2) turns into its supercritical state when pressure and temperature exceeds 73.8 bar and 31.1℃, correspondingly.[27] At this condition, the fluid has unique properties, where it does not condense or evaporate to form a liquid or gas. Instead, liquid and gas coexist in equilibrium as a single phase. At liquid-like densities $scCO_2$ exhibits low viscosity and high diffusion rates, just like a gas. It can diffuse through solid like a gas, and dissolve

materials like a liquid, acting as an efficient solvent in most polymers. In addition, the products usually possess high porosity, and the pore morphologies can be controlled by varying $scCO_2$ pressure or temperature. PS was chosen for the present study since our research group has extensive experience in the coating of CI microparticles with PS shell layer. In this paper, PS foam of the composite particles was prepared using $scCO_2$ fluid as a physical blowing agent via a rapid depressurization method.[28]

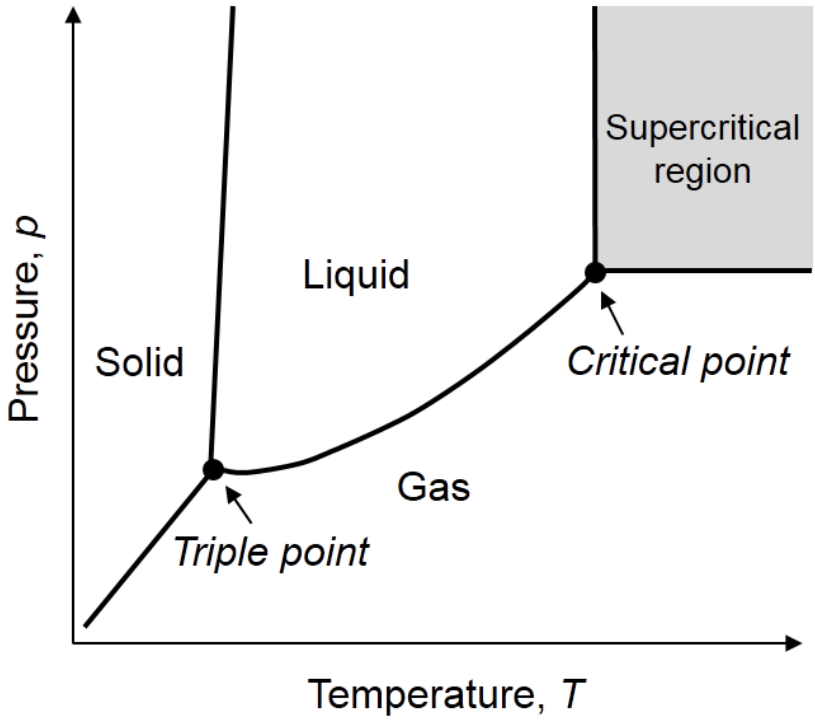

Figure 1. Phase diagram for carbon dioxide. Beyond a specific temperature and pressure (the critical point) carbon dioxide becomes a supercritical fluid, a state that neither is a gas nor a liquid, but has properties of both.

Figure 2 shows the fundamental foaming mechanism that governed the volume expansion behavior of a polymer foam. As aforementioned, the polymer foam is made up of a solid and gas phase mixed together to form a foam. The foaming process starts from a finished polymer bead (PS), which is foamed up in a separate step. In general, the polymer bead is saturated with CO_2 at a relatively high temperature and pressure (commonly, supercritical condition) followed by the rapid depressurization to atmospheric pressure. During the pressure quench, the polymer-and-gas mixture becomes highly supersaturated with CO_2 fluid, causing bubble nucleation and cell growth. The sample is allowed to soak for a set time to reach desired equilibrium state, and then is rapidly vented to atmosphere within few seconds. The drop in pressure will cause the gas to evaporate and polymer-fluid phase separate, foaming the polymer bead ─ leaving a cellular structure vacancy in the polymer phase. Since this generally happens too fast for the system to respond, CO_2 gas diffused into the polymer matrix is able to be trapped inside.[28]

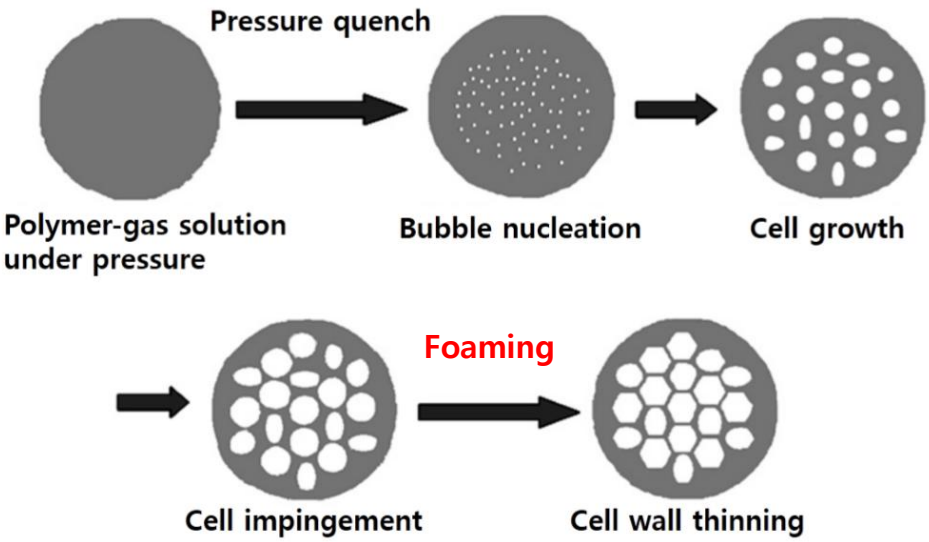

Figure 2. Schematic diagram of the foam generation process.

1.5 Objectives

The primary objective of the current work is to reduce the density of CI particles by the foaming of PS polymeric shell coated on the surface of CI particles. It is believed that through foaming process, the remarkable magnetic capability of the particles can be sustained meanwhile with a perceptible drop in density, owing to the dramatic increase in volume of polymer foam while the mass of particles is preserved. In this work, core-shell architecture was employed to synthesize CI coated with PS (CI/PSC) particles, in which the core-shell structure composed of inorganic CI micron-particle as core and PS as polymeric shell. As the first step, PS beads were deposited on the surface of CI particles through the conventional dispersion polymerization. After polymer coating, the density of CI particles decreased for about 5% and this implies that the volume of particles has increased as PS wrapped on them. Subsequently, the second step was introduced, the original sample of CI/PSC particles ─ with density reduction of 5% ─ was treated through $scCO_2$ fluid in which the foaming process happened, and then producing the sample of CI coated with PS foam (CI/PSF) micron-particles. After foaming, the density of CI/PSF sample declined as much as 35%, which indicates that the volume of particles has increased as PS shell becomes polymer foam. Finally, a number of characterizations were evaluated, including MR flow analysis; particles

element analysis; particles morphology; particles surface area; saturation magnetization; and sedimentation stability of MR fluids based on pure CI suspensions, CI/PSC suspensions and CI/PSF suspensions, and a comparison of the results was conducted.

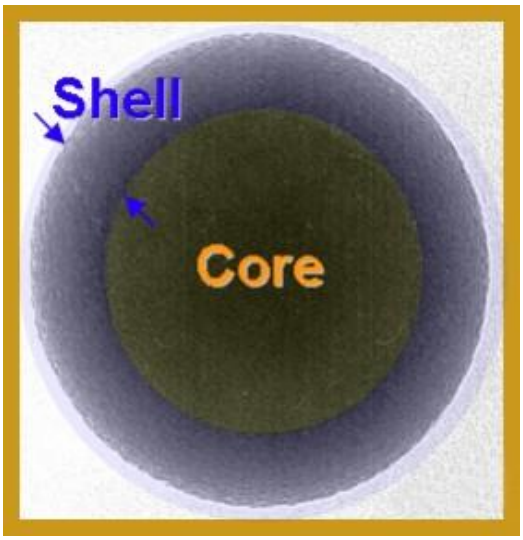

Figure 3. Core-shell structure particle.

The major advantage of foaming CI/PSF particles over coating CI/PSC particles are evidently proven with the greatly reduced density. Remember that density is defined as mass divided by volume. In order to achieve the low density similar to foaming particles by using only coating method, it needs many polymers to coat/attach on the CI particle surfaces to increase the volume of the particle. Note that polymer has its own mass too and a thick coating increases the mass of the coated particle, which even requires thicker coating to balance the mass added by expanding an extra volume. As a result, the particle possesses an extremely thick polymer shell and it is heavy. On the other hand, the reduction of particle density can be simply realized by foaming the polymer shell. The forming of polymer shell can enormously increases the volume of the particle, while the amount of coating (the mass of polymer coating) remains the same. At the same density, the particle produced using foaming method is certainly lighter than the one produced using only coating method. Also, the foaming particle has a thinner shell thickness (polymer coated on the particle surface) than the coating only particle. Consequently, at the same density, the foaming particle will definitely have a better MR performance than the coating only one due to its thinner shell and lower particle mass. This result is another significant outcome from this research.

CHAPTER 2. MATERIALS AND METHODS

2.1 Synthesis of CI Coated With Polystyrene (CI/PSC) Particles

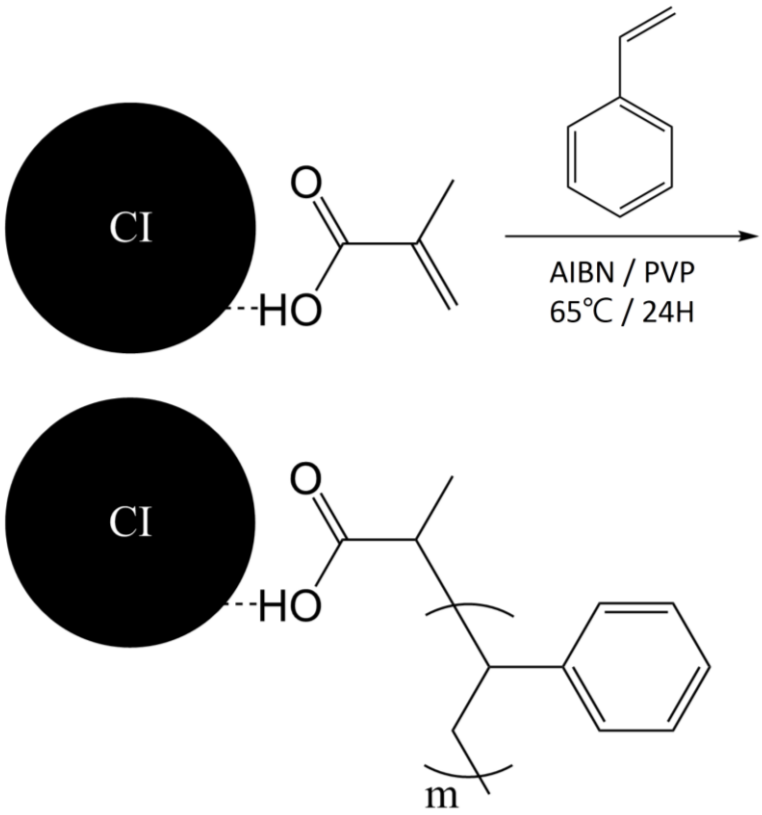

Figure 4. Schematic diagram of the synthesis of CI/PSC particles.

At first, the CI coated with Polystyrene (CI/PSC) particles were synthesized using a conventional dispersion method. A schematic diagram of the synthesis process for fabricating CI/PSC composite particles is illustrated in Figure 4.

The surface modification of CI particles was performed with a grafting agent so as to improve the affinity between metallic magnetic CI particles and the organic Polystyrene (PS) shell coating. The versatile functional grafting agent ─ Methacrylic Acid (MAA) ─ possesses two functional groups, which are carboxyl functional group and vinyl group. The carboxyl group, which is comprised of a hydroxyl group bonded to a carbonyl group, is used to modify the surface of the CI particles and attach entire MAA molecules onto the particle surfaces. So, the carboxyl group functions as an adhesive and grafts onto the CI particle surfaces, while the vinyl group reacts with the vinyl radical of the styrene monomer, leading to a successful polymerization of PS on the surface of CI particles.

Initially, magnetic CI particles (20 g) (CC grade, BASF, Ludwigshafen, Germany) were treated with MAA (99% purity, Junsei Chemical, Tokyo, Japan) by dispersion in a mixture solution of MAA (20 g)/methanol (200 g). In order to increase the interaction between CI particle surfaces and MAA molecules, the mixture was vigorously agitated using homogenizer at 9000 rpm for 5 minutes, following by ultrasonification for 5 minutes. The mixing process was repeated for 3 times. After 30 minutes, the excess MAA was removed by washing with additional methanol. A homogenous solution of Polyvinylpyrrolidone (13.2 g) (PVP; M_w = 1,300,000 g/mol, Sigma Aldrich,

USA) as a stabilizer in methanol (400 g) was prepared in a double-layered glass reactor (700 mL) fitted with a mechanical stirrer and a reflux condenser. Subsequently, the MAA-modified CI particles were placed into the reactor, and the mixture of MAA-modified CI particles and the PVP/methanol solution was stirred at 300 rpm for 30 minutes. After that, styrene monomer (20 g) (99% purity, Samchun Chemical, Korea) containing the initiator, Azobisisobutyronitrile (0.2 g) (AIBN; Junsei Chemical, Tokyo, Japan) was added slowly into the reactor. The system was then heated to 65℃ and maintained at the same temperature for 24 hours under 300rpm stirring. A high stirring rate was sustained to avoid sedimentation due to high density of CI particles. When the polymerization was complete, the final product was washed with excess methanol and distilled water several times to remove PVP or exceed PS oligomers. Finally, the resulting CI/PSC particles were dried in a vacuum oven at 60℃ for 24 hours.

2.2 Synthesis of CI Coated With Polystyrene Foam (CI/PSF) Particles

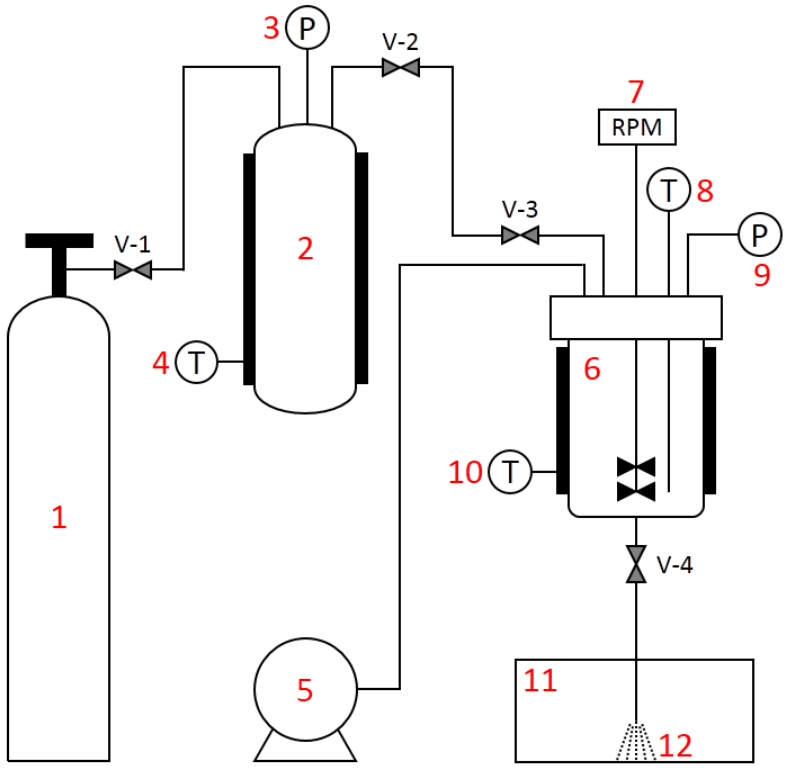

Figure 5. Schematic diagram of the $scCO_2$ foaming experimental setup for the foaming processing: (1) CO_2 gas cylinder, (2) sub chamber (3) pressure gauge, (4) heating unit with temperature indicator, (5) pump, (6) reaction chamber, (7) motor, (8) temperature indicator, (9) pressure gauge, (10) heating unit with temperature indicator, (11) container, (12) foaming product, and (13) V-1~V-4 valve.

The foaming of PS coating layer of CI/PSC particles was conducted using $scCO_2$ fluid as a physical blowing agent via a rapid depressurization method. The PS coating layer of CI/PSC particles was foamed as described above, and a PS foam coating layer that still remains on the surface of CI particles was obtained. The core-shell structure composed of inorganic CI particle as core and PS foam as polymeric shell was preserved. This final product is designated simply as CI coated with Polystyrene Foam (CI/PSF) particles.

A schematic diagram of the $scCO_2$ foaming experimental setup for the foaming of PS coating layer of CI/PSC particles is presented in Figure 5. The foaming machine was purchased from UTO Engineering Co., Ltd., Korea. Firstly, distilled water (130 mL) was poured into the high-pressure stainless steel vessel (400 mL) ─ reaction chamber and the dispersing agent, magnesium carbonate basic, heavy (13g) ($(MgCO_3)_4Mg(OH)_2 \bullet 5H_2O$; Dae Jung Chemical, Korea) was added and then mixed thoroughly. The dispersing agent, $MgCO_3$, acts to stabilize particles dispersion and prevent aggregation. Subsequently, CI/PSC particles (10 g) was dispersed in the mixture and agitated vigorously at 700 rpm. The reaction chamber was sealed carefully and the air in the reaction chamber was partially removed by a vacuum pump to a pressure of approximately 0.1 bar. After that, the vessels (both sub chamber and reaction chamber) was pressurized with CO_2 (99.98%

purity, Shin Yang Oxygen Ind. Co., Ltd., Korea) and heated in a manner as follows. Both vessels were heated up from 30℃ to 110℃ in 27 minutes then from 110℃ to 128℃ in 30 minutes. The sub chamber was used to build up the pressure of CO_2 gas when heated, and to regulate the desired pressure for the foaming process. After 57 minutes, the reaction chamber was again charged with scCO_2 up to the desired pressure by means of the sub chamber. The system was kept at that pressure (usually 140~150 bar) and temperature (128℃) for 1 hour. At the end of this period, the reaction chamber was depressurized rapidly by opening a fast discharge valve (V-4) and venting the mixture (scCO_2/distilled water/$MgCO_3$/sample) to atmosphere. The CI/PSF sample was collected in a container and washed with excess distilled water using a magnet to retain the particles. Lastly, the final product CI/PSF particles were dried completely in a vacuum oven at 60℃ for 24 hours.

2.3 Characterization Methods

The samples were used as a very fine powder, if possible, by grinding it in a mortar. The densities of pure CI particles, CI/PSC particles, CI/PSF particles were measured using a helium pycnometer (AccuPyc 1330, Micromeritics Instrument Corporation, Norcross, GA). The surface morphologies of the pure CI particles, CI/PSC particles, and CI/PSF particles were observed using scanning electron microscopy (SEM; SUPRA 55VP, Carl Zeiss, Germany). The elemental analysis was obtained from the X-ray energy dispersive spectra (EDS) using an attached EDAX (coupled with SUPRA 55VP) spectrometer. The specific surface areas of each sample were determined by Brunauer–Emmett–Teller (BET) adsorption measurements on a Micromeritics TriStar analyzer (TriStar 3000, Micromeritics Instrument Corporation, Norcross, GA). The saturation magnetization of the particles is an important parameter on the MR properties. Each sample in powder state was inserted into a capsule and the saturation magnetization was checked by a vibrating sample magnetometer (VSM; Model 7307, Lake Shore Cryotronics, Westerville, OH).

MR fluids for each sample were prepared by dispersing the particles in the silicone oil (KF-96, 50cS, Shin Etsu, Japan) at a particle concentration of 20 vol%. The rheological properties of the MR fluids were investigated using

a commercially available rotational rheometer (Physica MCR 300, Stuttgart, Germany) equipped with a magnetic field generator (Physica MRD 180). The magnetic field direction was set perpendicular to the flow direction. A parallel-plate measuring system with a diameter of 20 mm was employed at a gap distance of 1 mm. The parallel-plate measuring system is made of non-magnetic metals to prevent occurrence of radial magnetic force components on the shaft of the measuring system. Also, all of the tests were performed at room temperature. An optical microscope (Olympus BX-51, Japan) was used to observe the response of CI-based MR fluids when exposed to an externally applied magnetic field in the microscopic level. Finally, the sedimentation stability of the suspensions was analyzed via Turbiscan (Classic MA2000, Formulation, France). In this experiment, MR fluids at a particle concentration of 10 vol% were tested. The device scanned the cell height (in μm) periodically and recorded the light transmission profile that varied with the cell height over time upon the sedimentation of the particles. Then these information collected was interpreted as the percentage of transmission as a function of time to indicate the stability of the suspension.

CHAPTER 3. RESULTS AND DISCUSSION

The premise of the present study is to tailor core-shell structured CI with PS Foam (CI/PSF) microparticles using $scCO_2$ foaming processing, creating CI/polymer foam composite particles with lower density for enhancing their sedimentation stability in MR suspensions. Dual-step processing was employed to first introduce a PS coating layer on the CI particle surfaces following by the foaming of the PS coating layer. More importantly, the effects of these processing on the magnetic properties, MR behaviors, sedimentation stability and particle surface morphologies were inspected and comparisons were done between the modified (coating and foaming CI) and the control (pure CI) samples.

3.1 Density After Coating and Foaming Processing.

The CI particles after coating and foaming modification show a change in their density and the variation is given in Table 1. It is clear that the density for pure CI is 7.80 g cm^{-3} which is the highest among others. Pure CI particles are the bare CI particles purchased from BASF chemical company and before undergoing any modification. Upon the coating of PS shell on CI particles, the CI/PSC particles display a reduction in their density from 7.80 g cm^{-3} to

7.56 g cm^{-3} (about 3.1% decrease) for sample B, CI/PSC (7.56) and 7.34 g cm^{-3} (5.9% decrease) for sample C, CI/PSC (7.34), respectively. By changing the mole ratio of reactants, it is possible to control the amount of PS coated on CI particles, thereby the density of CI/PSC particles can be easily controlled. Subsequently, after the coating CI/PSC particles were processed through the $scCO_2$ foaming, the density has further been reduced from 7.56 g cm^{-3} to 6.36 g cm^{-3} (approximately 18.5% decrease) for sample B1, CI/PSF (6.36), and from 7.34 g cm^{-3} to 5.10 g cm^{-3} (34.6% decrease) for sample C1, CI/PSF (5.10). In the $scCO_2$ foaming process, each sample went through the foaming condition as shown above in Table 1. The results of the present study correspond well with those found in the earlier experiment studies in polymer coating of CI particles.

Among those five samples stated above, four samples have been systematically studied in the current work, which are sample A, pure CI (7.80); sample C, CI/PSC (7.34); sample B1, CI/PSF (6.36); and sample C1, CI/PSF (5.10).

Table 1. Density of CI particles after coating and foaming processing.

No.	Samples			Foaming Condition	Density [g cm^{-3}]
	Control	Coating	Foaming		
A	Pure CI	–	–	–	7.80
B	–	CI/PSC	–	–	7.56
B1	–	–	CI/PSF	128℃ / 141 bar	6.36
C	–	CI/PSC	–	–	7.34
C1	–	–	CI/PSF	128℃ / 144 bar	5.10

3.2 Particles Surface Morphologies, Chemical Composition, and Specific Surface Area.

3.2.1 Scanning Electron Microscopy (SEM)

The particle morphology was investigated for each sample. SEM images of the (a) pure CI, (b) CI/PSC (7.34), (c) CI/PSF (6.36) (the inset shows a magnified view of the particle surface), and (d) CI/PSF (5.10) are depicted in Figure 6. The pure CI particles, shown in Figure 6a, had smooth surfaces and a polydisperse size distribution. It is obvious, from Figure 6b, that formation of the PS polymer brought distinct changes in the surface morphology. The CI particles were covered by many PS nanobeads with polydisperse size distribution. The surface of CI/PSC (7.34) particles was rough, unlike the smooth surfaces of the pure CI particles. This implies that the PS polymer was coated successfully onto the CI particles and the presence of grafting agent MAA have made it feasible to achieve coating over the particle surfaces. PS nanobeads formed in the dispersion polymerization at the high mechanical stirring rate. This trend can be explained by the energy transfer differences for the different stirring rates as increasing the stirring rates has increased the energy transferred to the suspension medium which caused the reaction solution (styrene monomers) to disperse into smaller droplets and produced nano-sized polymer beads. Under a vigorous agitation, these PS nanobeads

had high possibility to collide with neighboring CI particles and attached onto their surfaces. Other possibilities may include the use of grafting agent MMA that triggered those PS nanobeads tend to react with their vinyl functional active sides, and the stabilizer, PVP, also affected the development of this structure.[23] Figure 6c and 6d show the surface morphology of CI/PSF (6.36) and CI/PSF (5.10) particles obtained after the $scCO_2$ foaming processing. In Figure 6c, the inset is the zoom-in view of the CI/PSF (6.36) particle surface at magnification x200,000. A mass of polystyrene nanospheres were compactly spread over the surface of CI/PSF particles. Correspondingly, the CI/PSF (5.10) particles also appeared to have an analogous surface texture. The particle surfaces for both CI/PSF (6.36) and CI/PSF (5.10) particles were noticeably rougher than for pure CI or CI/PSC (7.34) particles. Undoubtedly, the spherical shape of both CI/PSF particles was preserved as are shown in the SEM images.

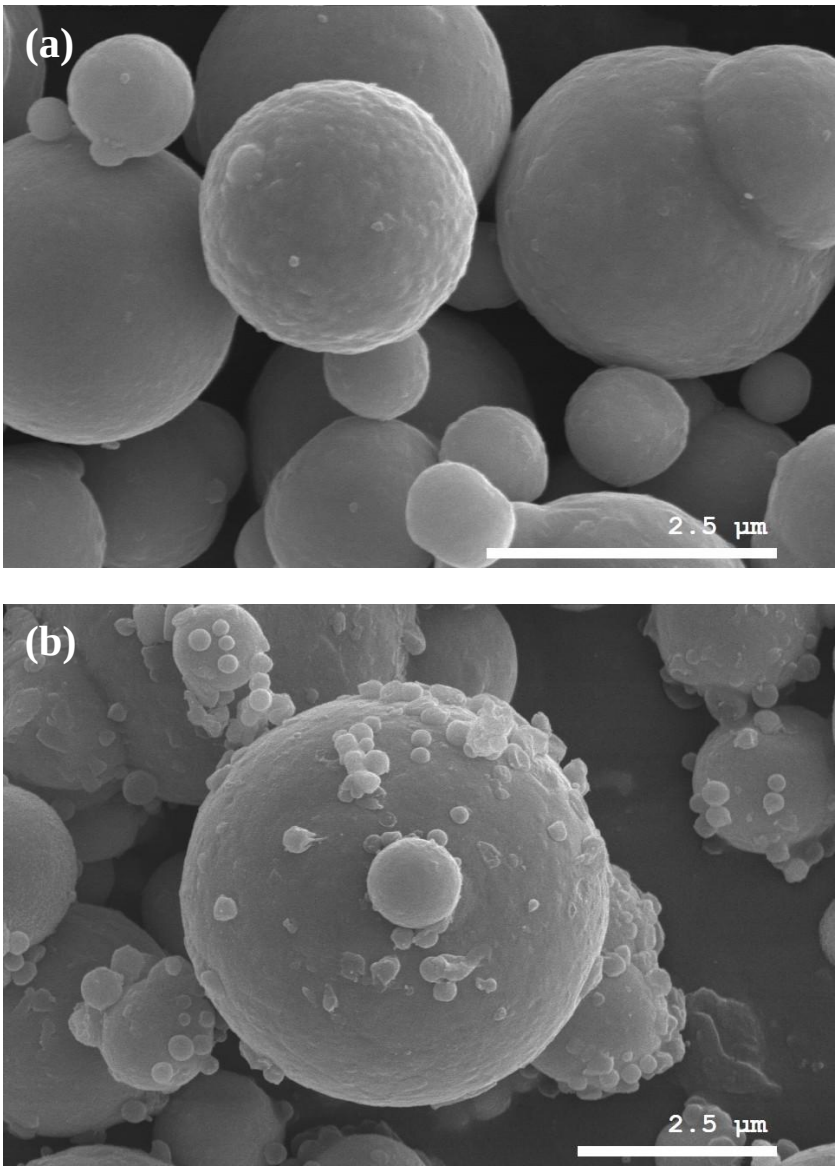

Figure 6. SEM images of the (a) pure CI, (b) CI/PSC (7.34), (c) CI/PSF (6.36) (the inset shows a magnified view of the particle surface), and (d) CI/PSF (5.10).

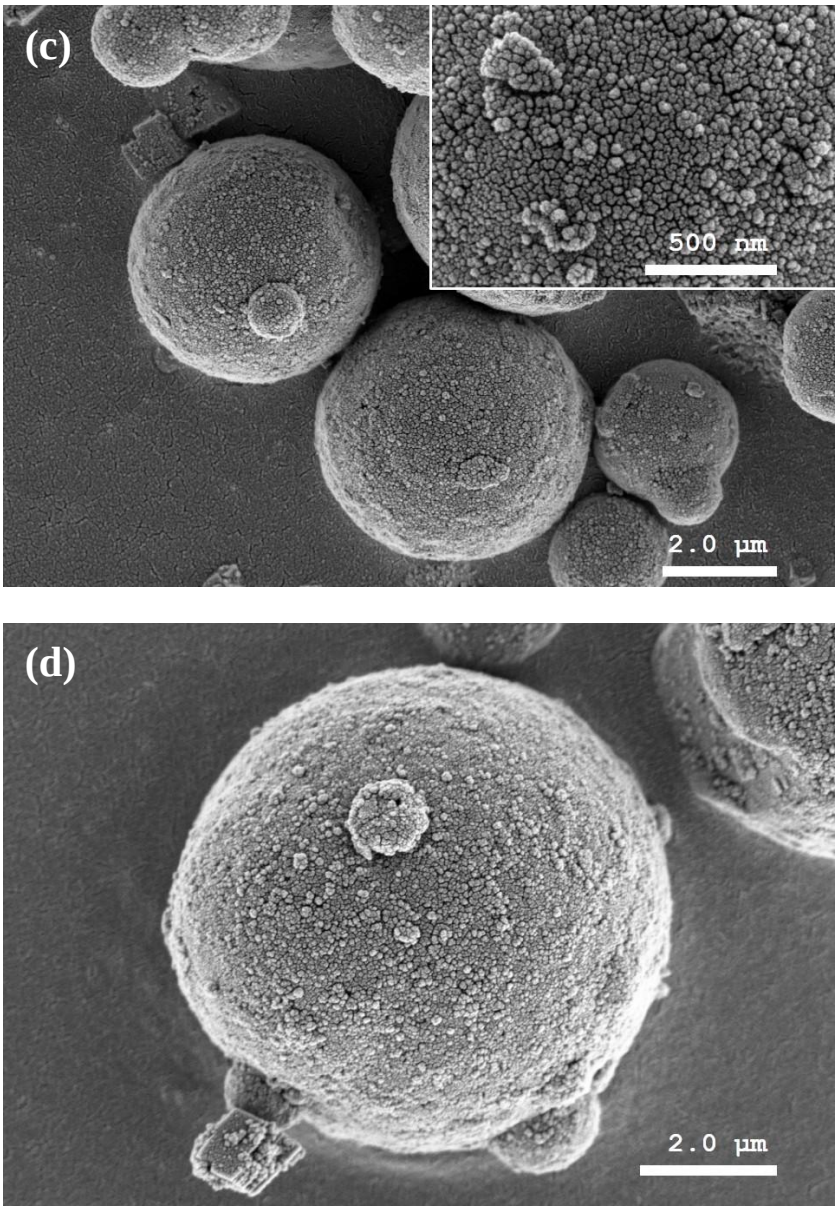

Figure 6. SEM images of the (a) pure CI, (b) CI/PSC (7.34), (c) CI/PSF (6.36) (the inset shows a magnified view of the particle surface), and (d) CI/PSF (5.10).

3.2.2 Energy-dispersive X-ray Spectroscopy (EDS)

In the $scCO_2$ foaming process to synthesize CI/PSF particles, the dispersing agent, $MgCO_3$, was added to stabilize particles dispersion and prevent aggregation.[29] As $scCO_2$ fluid diffused into the PS polymer, the fluid molecules accumulated interstitially between the polymer chains, increasing the free volume and mobility of the polymer chains. In this capacity the $scCO_2$ fluid acted as a plasticizer, and as such lowered the glass transition temperature (T_g) of the PS polymer.[30,24] The colloidal particles were prone to aggregate upon contact and difficult to be separated again. In order to verify that $MgCO_3$ did not contaminate the samples, the EDS element analysis was carried out. A specific region on the surface of a CI/PSF particle was selected to determine the chemical composition of its surface, as presented in Figure 7. The result in Table 2 indicates that the CI/PSF (5.10) sample consists of 90.19 wt% of Iron, 7.13 wt% of Carbon and 2.68 wt% of Oxygen. It is inferred that no dispersing agent $MgCO_3$ remains after washing and was well removed from the samples after the foaming process. In additional, there is enough evidence to prove that the increased intensity of C and O organic species combined with a decreased intensity of Fe, demonstrated that the CI particles were successfully coated with a PS shell. Last but not least, we postulate that the CI particles were not oxidized or only fairly oxidized during the foaming process as there is just

small amount of Oxygen presents in the sample. Besides, it is possible that some of the oxygen element may come from MAA's carboxylic group.[23]

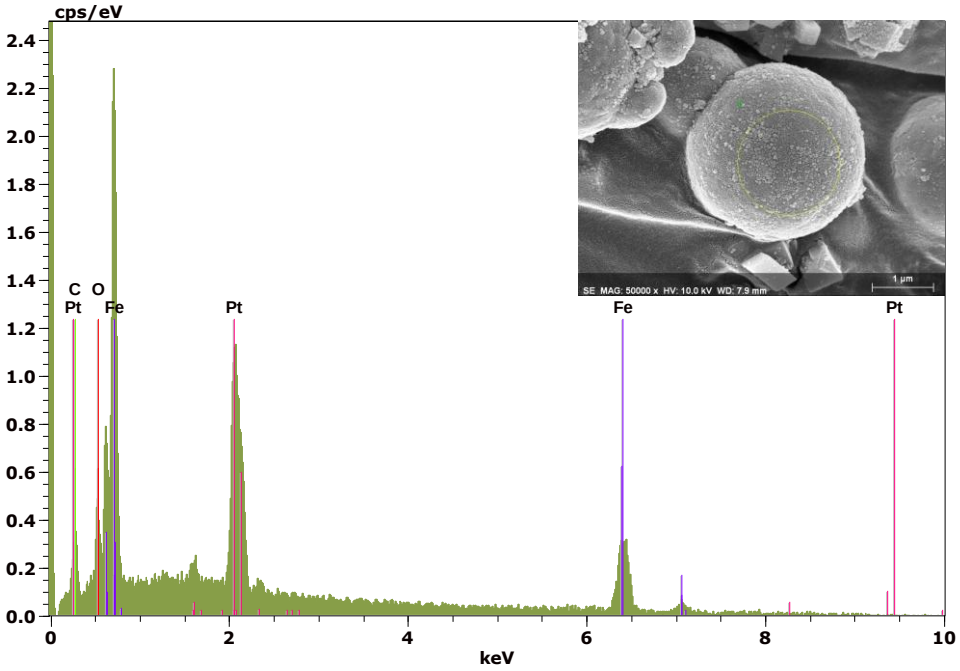

Figure 7. CI/PSF (5.10) particle with EDS spectra.

Table 2. Element Composition of CI/PSF (5.10) Particles.

Element	Weight Percent (wt%)	Atomic (%)
Iron (Fe)	90.19	67.96
Carbon (C)	7.13	24.98
Oxygen (O)	2.68	7.06

3.2.3 Brunauer–Emmett–Teller (BET) Specific Surface Area

We can observe surface roughness due to voids, pores, steps, and other surface imperfections via BET adsorption measurement as these surface irregularities always create a new surface area. The determination of specific surface areas and BET C values from the BET theory is a straightforward application of the BET equation, which is stated as below.

$$\frac{1}{Q(P_0/P-1)} = \frac{1}{Q_m C} + \frac{C-1}{Q_m C}\left(\frac{P}{P_0}\right)$$

By substituting the data provided in the BET plot, as shown in Figure 9, into the BET equation, calculations were made to find the specific surface areas and BET C values. For your reference, the results of specific surface area and BET C value for each sample are listed in Table 3. The values of specific surface area as high as 0.1907 m^2 g^{-1}, 0.2433 m^2 g^{-1}, and 0.7255 m^2 g^{-1} were obtained for pure CI, CI/PSC (7.34) and CI/PSF (5.10) particles, respectively. Figure 8 and 9 shows the sorption isotherms and BET plots for pure CI, CI/PSC and CI/PSF particles.

As can be seen from Table 3 and Figure 8, all 3 samples possess the type 2 sorption isotherm. A type 2 sorption isotherm indicates that the surfaces are non-porous or macroporous (pore of internal width greater than 50 nm). It

appears that specific surface area increased after coating and foaming modification, however, there is no prominent increases in the value (3.8-fold increase). In fact, the range of specific surface area can vary extensively depending on the particle's size, shape, and porosity. The influence of pores can often overwhelm the size and external shape factors. Particles contained extensive porosity can eventually exhibit extremely high specific surface area values. So, it is inferred that their surfaces were non-porous with different roughness. Or in the case of foaming particles, only some macroporous cavity existed on its surfaces. Moreover, this result can further confirm that the foaming processing has increased the porosity on the surface of CI/PSF particles. The PS foam shell of CI/PSF particles possesses many cavities, contributing to a rough surface that helps to retard the sedimentation.

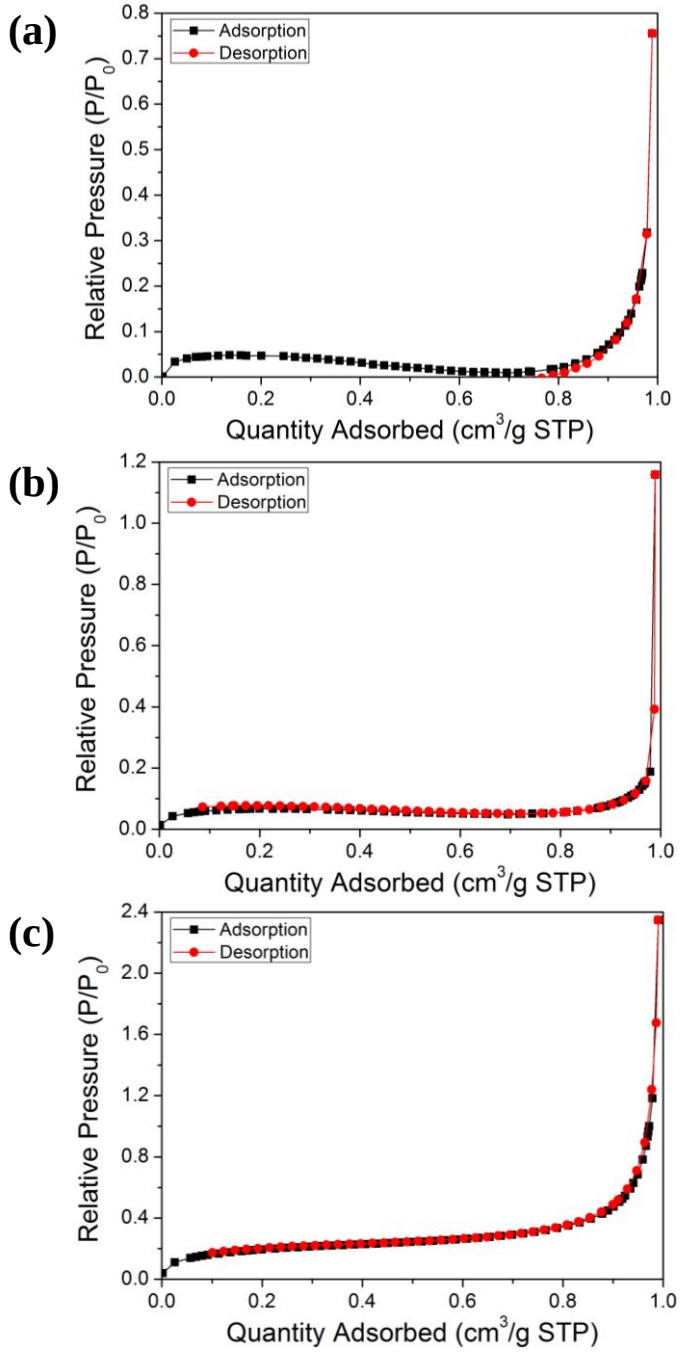

Figure 8. Sorption isotherms of (a) pure CI, (b) CI/PSC (7.34), and (c) CI/PSF (5.10) particles.

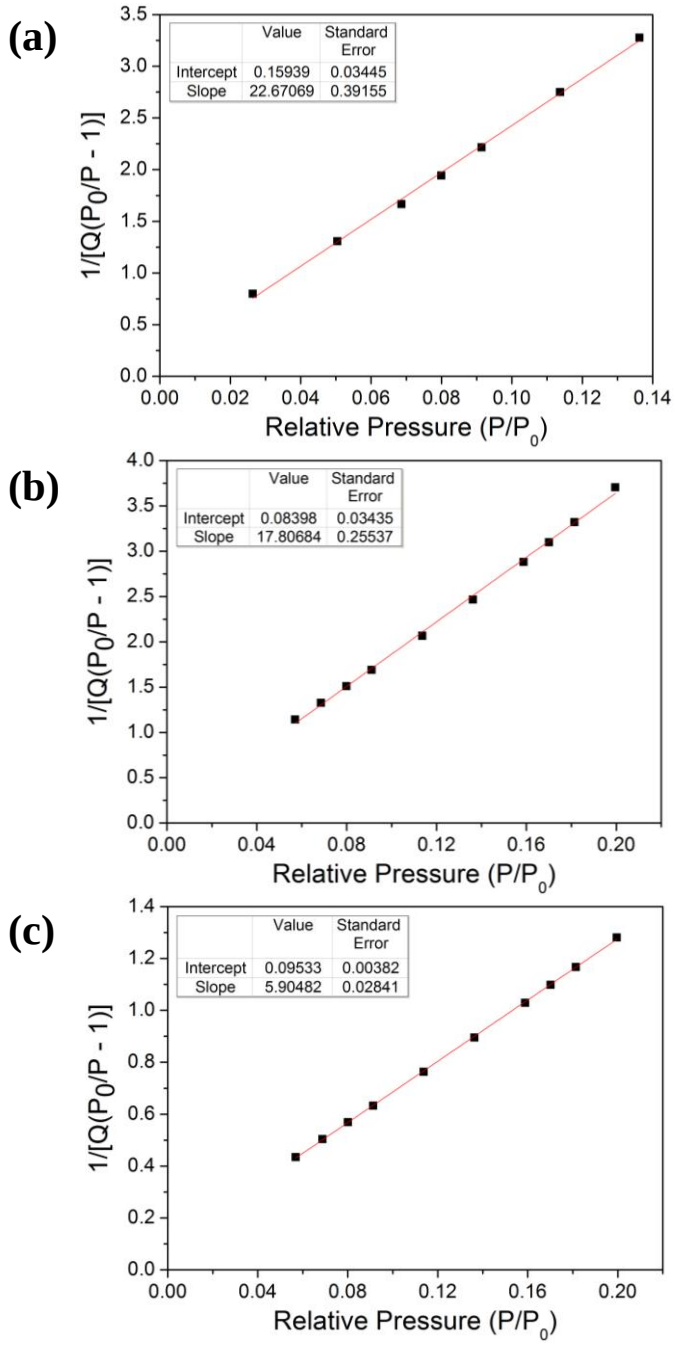

Figure 9. BET plot of (a) pure CI, (b) CI/PSC (7.34), and (c) CI/PSF (5.10) particles.

Table 3. Specific surface area and BET C value obtained using BET equation for pure, coating and foaming CI particles.

Samples	**Specific Surface Area, $a_{s,BET}$ [m^2 g^{-1}]**	**BET C value**
Pure CI	0.1907	143.2378
CI/PSC (7.34)	0.2433	213.0482
CI/PSF (5.10)	0.7255	62.9401

3.3 Magnetic Properties.

The magnetic hysteresis loops of the pure CI particles, CI/PSC (7.34) particles, CI/PSF (6.36) particles, and CI/PSF (5.10) particles in the powder state, measured in the magnetic field range from -10 to 10 kOe, are illustrated in Figure 10. The maximum possible magnetization, or magnetization saturation M_s, of each sample differed from one and another, but the intrinsic hysteresis behavior of the pure CI particles was maintained in that of CI/PSC (7.34), CI/PSF (6.36), and CI/PSF (5.10) particles. All four samples had only little magnetic hysteresis which means that these materials loss their magnetization instantly once the applied magnetic field is removed and this type of material is called soft magnetic material. The magnetization saturation value for the pure CI, CI/PSC (7.34), CI/PSF (6.36), and CI/PSF (5.10) particles were 184, 171, 147 and 112 emu/g, respectively. The CI/PSC (7.34) particles demonstrated a slight reduction in the magnetization saturation upon introduction of the nonmagnetic PS shell. Additionally, the magnetization saturation has decreased substantially following by the foaming process that brought to a tremendous expansion in the volume of PS shell. The presence of PS shell increased the separation distance between those magnetic particles which weakened their interaction force. These results are in close agreement with those of numerous authors.[22,31,32]

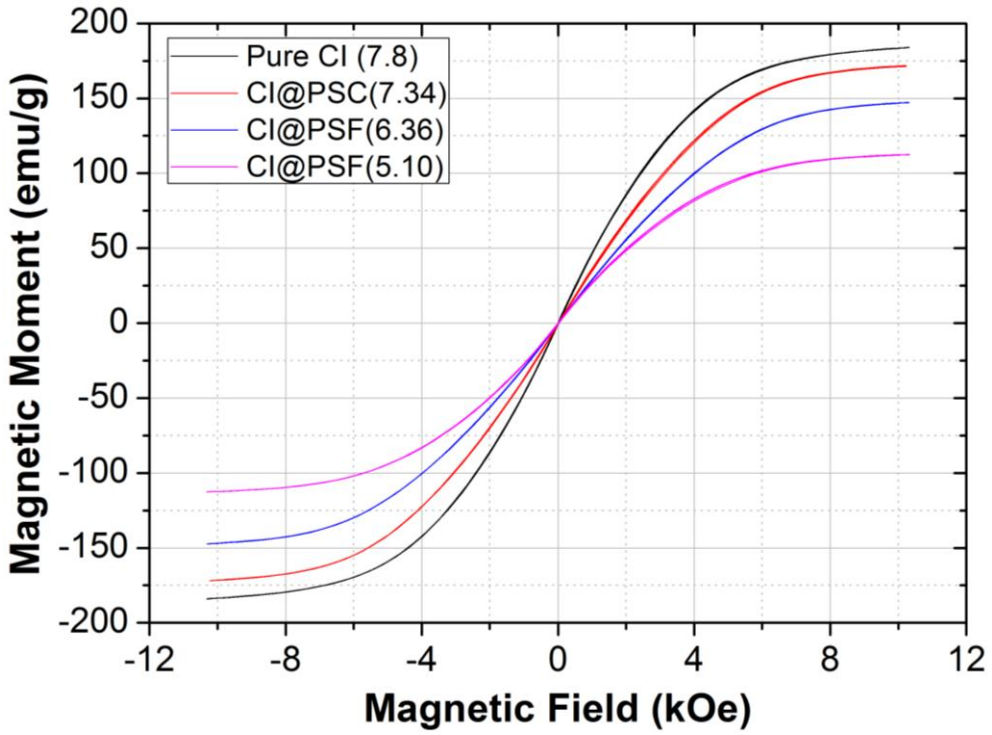

Figure 10. VSM data of the pure CI particles, CI/PSC (7.34) particles, CI/PSF (6.36) particles, and CI/PSF (5.10) particles.

3.4 Magnetorheological Properties.

Rheological evaluation of MR fluids is useful for understanding the transition from liquid-like to solid-like state upon the application of an externally exerted magnetic field.

3.4.1 Response to Magnetic Field

The fluid converts from liquid-like to solid-like state upon its exposure to a magnetic field because magnetic particles suspended in the fluid form fibril chain-like structures aligning along the applied magnetic field direction, and these column structures restrain the fluid from flowing by spanning the gap of a flowing channel.

Figure 11 illustrates the MR fluid before and after the application of an external magnetic field with the chain-like structures formed as the response to the stimuli of the magnetic field. Before the application of a magnetic field, magnetic particles dispersed in silicone oil are positioned randomly. Nevertheless, the particles line up along the magnetic field direction upon the application of a magnetic field. A simplified explanation for the development of the chain-like structure upon the exertion of magnetic field in MR fluids is as follows. Application of a magnetic field triggered the magnetic polarization

of each iron particle. As mentioned before, the magnetized particles attracted one another and built up chain-like structures aligned in the field direction. The magnetic dipoles induced in the particles led these chains to grow parallel to the applied field for the reason that in order to attain the state of minimum potential energy, particles tended to align along the direction of the external magnetic field.[7] Hence they formed chain-like structures as shown in Figure 11b.

Unfortunately, the microscopic mechanisms at work in the fluid are not at all clear. Scientists were trying to understand the underlying physics of MR fluids. NASA's InSPACE program has taken its MR fluid experiment on board the International Space Station to eliminate gravity and by doing so, it can eliminate the problem of sedimentation and gain a clearer idea of why particles in the fluid act as they do when exposed to rapidly alternating magnetic fields.

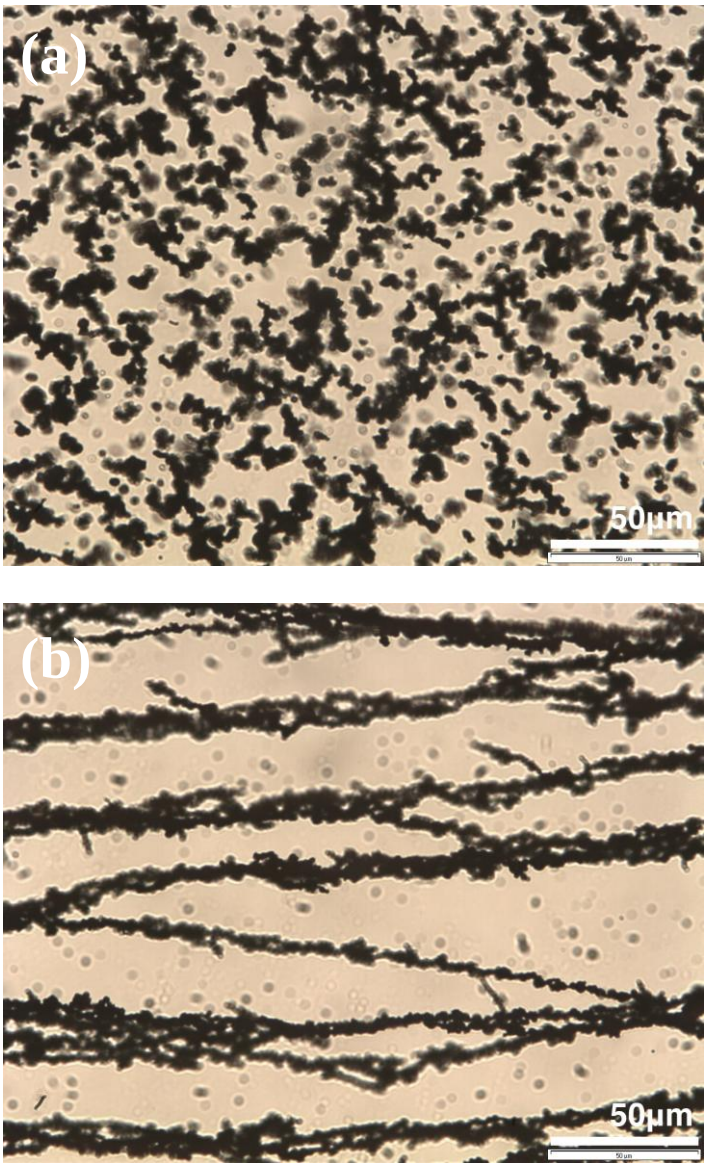

Figure 11. Optical Microscope images (at magnification x500) of microstructural change for the pure CI particles based MR fluid under an external magnetic field. The microstructure in the MR fluid (a) before and (b) after the application of an external magnetic field.

3.4.2 Amplitude Sweep Measurement

The oscillatory tests (amplitude and frequency sweep) were performed to investigate the viscoelastic behavior, along with the process of chain formation in MR fluids. Figure 12 demonstrates an amplitude sweep measurement that describes the changes of the storage modulus, G´ as a function of strain for pure CI, CI/PSC (7.34), CI/PSF (6.36) and CI/PSF (5.10) based MR suspension. Note that the storage modulus, G´ represents the elasticity of the MR fluid and loss modulus, G˝ denotes the viscous behavior of the MR fluid, respectively.[33] With increasing magnetic field, the storage modulus increased. Notice that there is a stable plateau in the graph that terminated at strain approximately 10^{-2}%. This region is identified as the linear viscoelastic region in which the storage modulus is independent of the applied strain. In this region, magnetic induced structures remain undisturbed. As the strain amplitude increases, the chain structure starts to break. The destruction of chains after the plateau region was irreversible. The storage modulus of the correlated MR fluids slightly decreased with the reduction in their density (from pure CI to CI/PSC (7.34), then CI/PSF (6.36), and lastly CI/PSF (5.10)). The deterioration of magnetization saturation of the particles after coating and foaming constructed a weaker chain structures under the applied magnetic field, which were less stiff to withstand the shear strain exerted to them. The

same phenomenon can be observed in the MR flow curve.

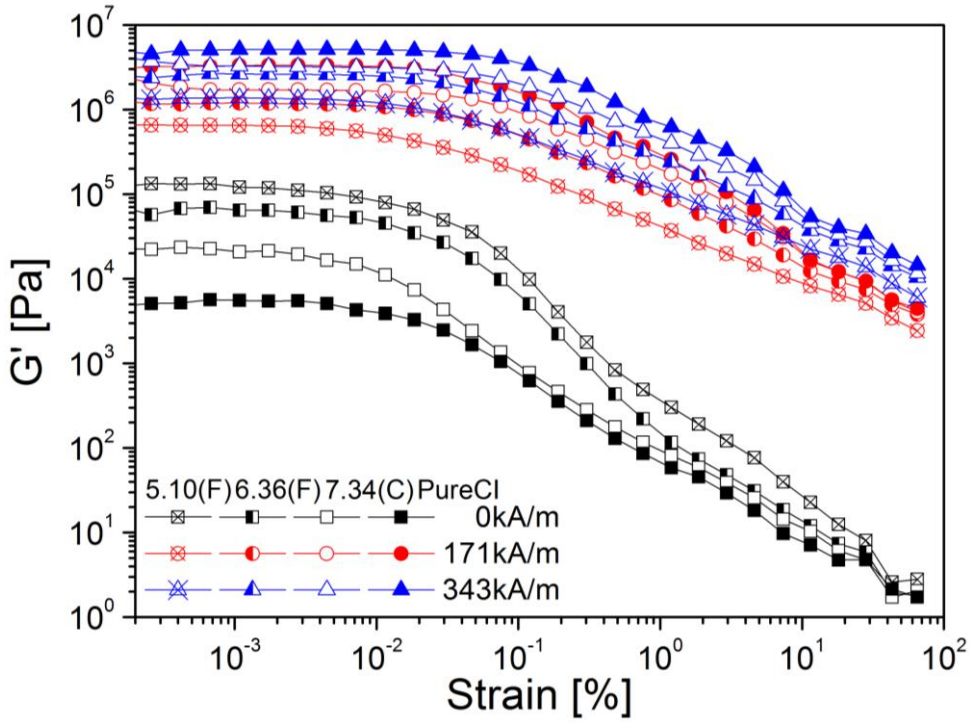

Figure 12. Amplitude sweep dependence of storage modulus, G´ for each MR suspension under various magnetic field strengths.

3.4.3 Frequency Sweep Measurement

From Figure 13 and Figure 14, they revealed that upon applications of the external magnetic field, both storage modulus, G′ and loss modulus, G″ increased in two to three orders of magnitude, respectively. This is because the chains were reinforced via a stronger dipole-dipole interaction between the neighboring magnetic particles with increasing magnetic field intensity. Moreover, storage modulus values in both graphs increases slightly as the angular frequency rises up, which shows the formation of chain structures that enable the transmission of elastic forces within the MR system in the presence of a magnetic field.

In general, all the storage modulus expressed by all three MR fluids are higher than their corresponding loss modulus (G′ > G″), which verifies the dominant solid-like elastic properties shown by the MR fluids upon their exposure to a magnetic field. In the absence of the external magnetic field, the storage modulus should be lower than the loss modulus (G′ < G″), and the viscous behavior predominated so that the fluid can behave more likely as liquid-like state.[34] However, our result is contrary to the theory.[35] In order to standardize every run and make sure it was kept in a constant condition, the demagnetization procedure was repeatedly done before every test began. We

postulate that after demagnetization, chain-like structures formed in the MR suspensions and these remained chain-like structures contributed to the solidification (solid-like) of the MR fluids as they always do once exposure to a magnetic field. Due to this reason, the MR fluids examined in the present work exhibited an elastic behavior (solid-like state) instead of viscous liquid state.

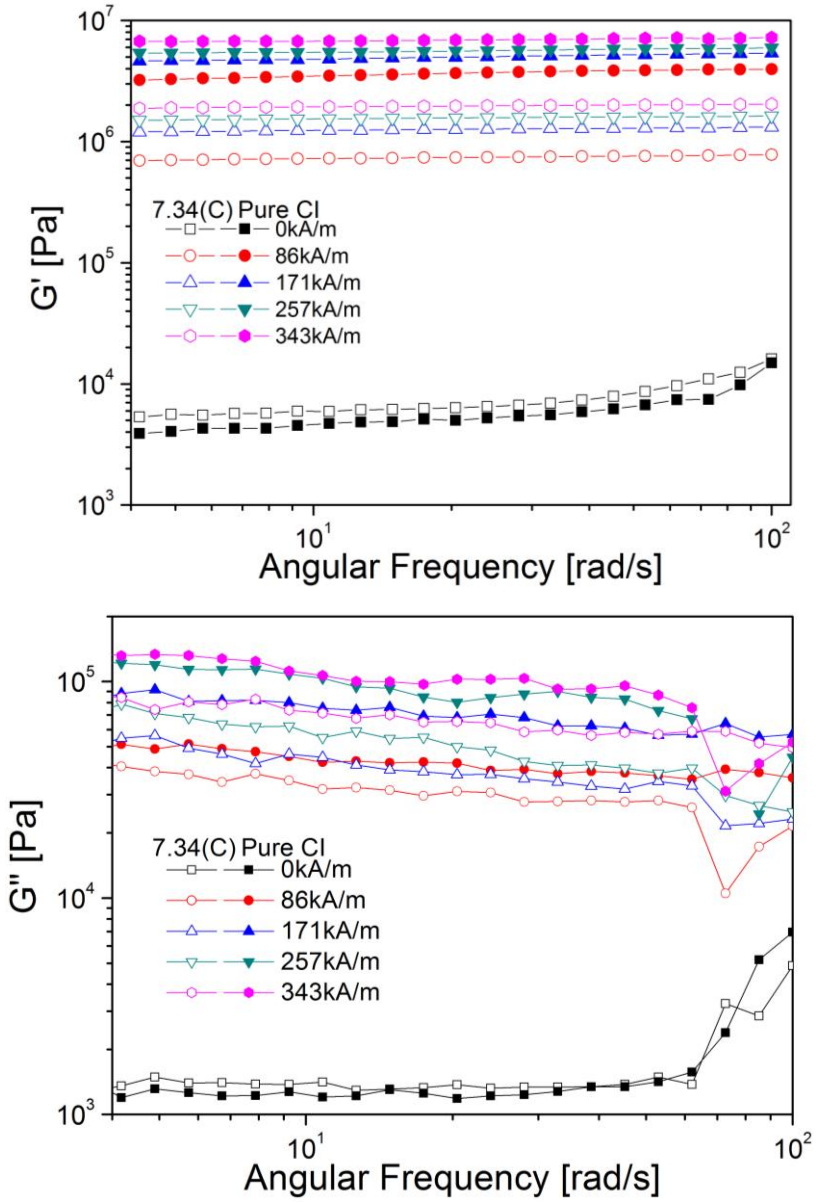

Figure 13. Frequency dependence of storage modulus, G′ and loss modulus, G″ for pure CI and CI/PSC (7.34) based MR suspensions under various magnetic field strengths.

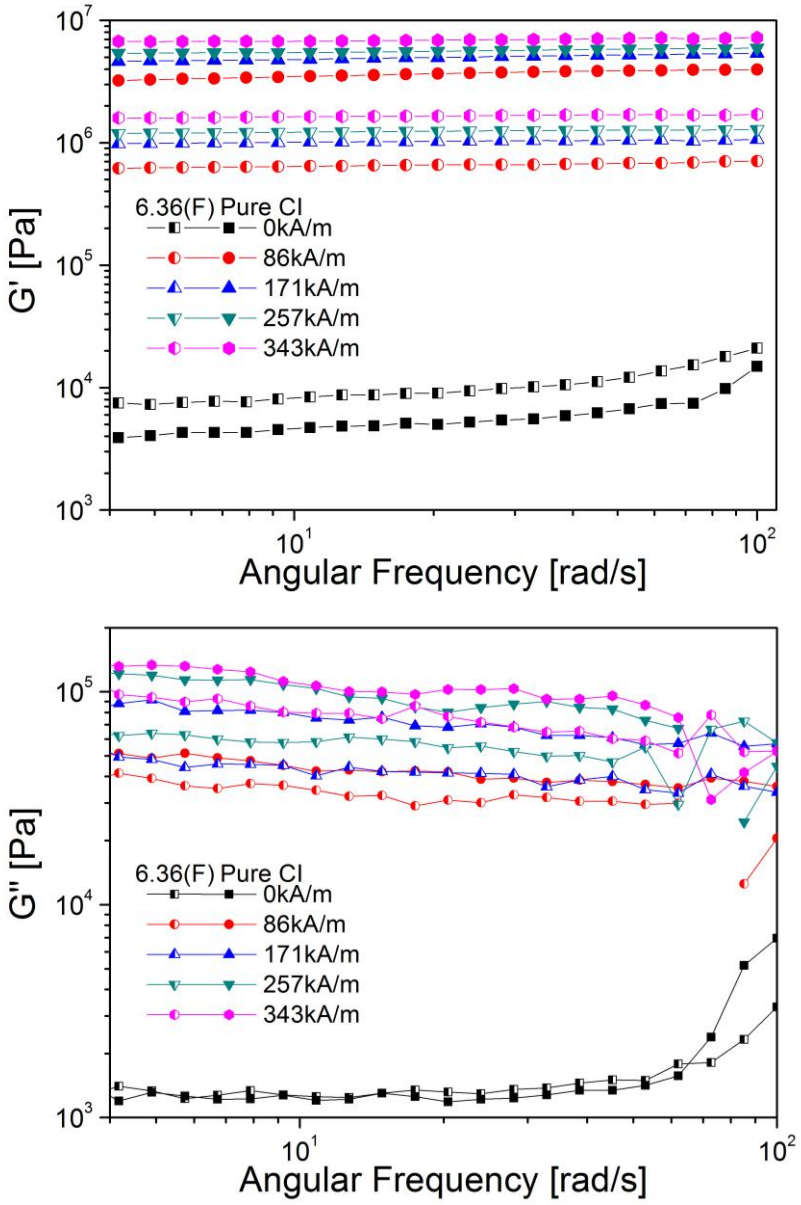

Figure 14. Frequency dependence of storage modulus, G′ and loss modulus, G″ for pure CI and CI/PSF (6.36) based MR suspensions under various magnetic field strengths.

3.4.4 Shear Stress Flow Curve

As shown in Figure 15, it revealed that the shear stress obtained had a strong dependence on the applied field strength, in which stronger magnetic field applied, higher shear stress performed by MR fluids. This observation was attributed to the robust particulate chain structures formed because of the strong dipole-dipole interactions between adjacent magnetic particles. It is obvious that the pure CI suspension had the highest shear stress, following by the CI/PSC (7.34) suspension, then CI/PSF (6.36) suspension and finally CI/PSF (5.10) suspension. This phenomenon can be explained using the VSM data that describes the magnetization saturation of each sample. This difference in the magnetization saturation was attributed to the presence of PS shell and the coating and foaming processing altered the thickness of shell. As volume expanded, it increased the distance between particles in the chain. The strength of magnetic interaction decreased roughly exponentially over distance. When an external magnetic field was applied, the magnetic particles become magnetized and behave like tiny magnets. Mehdizadeh *et al* has asserted that the magnetic interaction force (attraction force in our case) between magnetic particles diminished exponentially as the distance increased. The attraction force between two soft magnetic spheres is inversely proportional to the fourth power of the distance between the centers of the

particles.[36] Consequently, coating and foaming samples may have weaker magnetization performance because the saturation magnetization is a crucial factor for the superior MR effect. Under an applied magnetic field, the systems exhibited Bingham fluid behaviors. All four of the suspensions indicated a wide plateau region through the low and medium shear rate range. This wide plateau was attributed to the dipole-dipole interactions among adjacent magnetic particles. However, at high shear rate region, the viscosity term is dominant (viscosity term in Bingham plastic model) over the magnetic field induced shear stress to show the increase of shear stress with shear rate.[37,38]

Bingham fluids are Non-Newtonian fluids characterized by a yield stress, τ_y. The Bingham fluids begin to flow only when the shear stress is higher than the yield stress. Hence the fluids behave as a solid below the yield stress and as a liquid above the yield stress threshold. The relation between shear stress and shear rate for the Bingham fluid is as follows. Bingham plastic model, $\tau = \tau_y + \eta_{pl}\dot{\gamma}$, where τ is the shear stress, τ_y is the magnetic field-dependent yield stress, η_{pl} is the plastic viscosity, and $\dot{\gamma}$ is the shear rate.[3] The yield stress, τ_y is recognized as the dynamic yield stress.

Without a magnetic field, all suspensions displayed typical Newtonian behaviors. The CI/PSC and CI/PSF systems exhibited a slightly higher shear

stress than the pure CI suspension. This observation was predicted by analyzing the surface morphology of CI/PSC and CI/PSF particles. When an external shear field was exerted, a rough surface of particles might increase flow resistance to fluid medium. Therefore, the CI/PSF (6.36) and (5.10) based MR fluids demonstrated a higher shear stress than the CI/PSC and pure CI suspensions.[22] Also, the increase in particle volume after foaming led to a big particle size to the foaming samples and so it increased the hydrodynamics interaction with the carrier liquid.

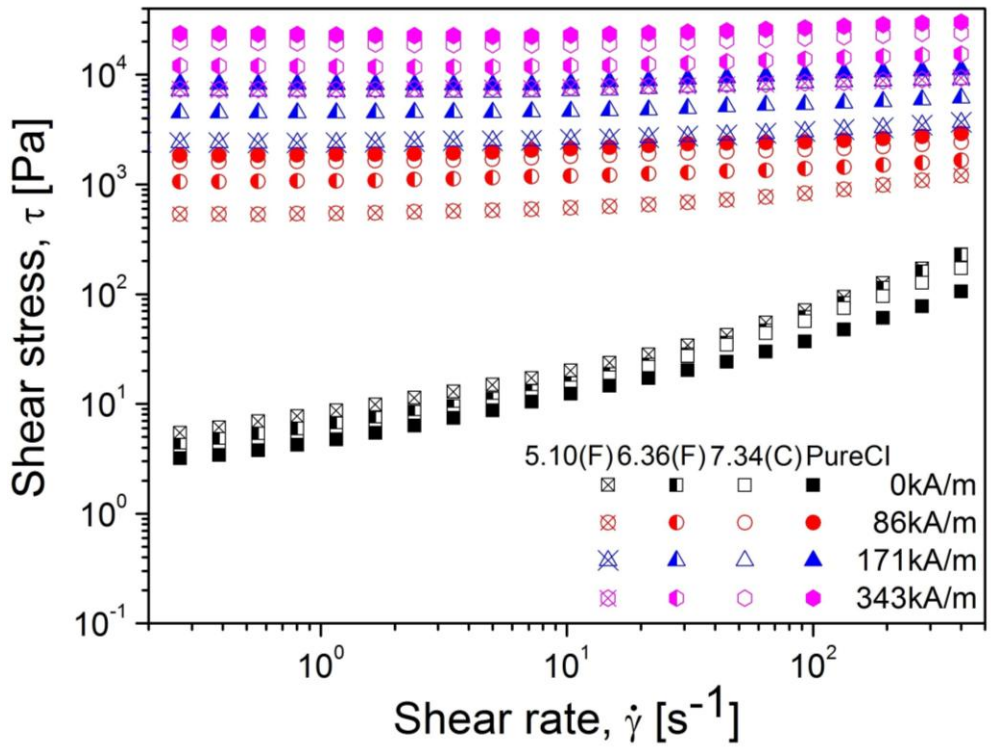

Figure 15. Shear stress flow curve for 20 vol% of pure CI, CI/PSC (7.34), CI/PSF (6.36), and CI/PSF (5.10) suspensions under different magnetic field strengths.

3.4.5 Shear Viscosity Flow Curve

Figure 16 shows the shear viscosity as a function of the shear rate for 20 vol% of pure CI, CI/PSC (7.34), CI/PSF (6.36), and CI/PSF (5.10) suspensions under different magnetic field strengths. As the shear rate increased, the viscosity of MR suspensions decreased linearly. This result indicated that four of these suspensions are shear-thinning fluid.[12] The shear rate, $\dot{\gamma}$, is the velocity gradient perpendicular the direction of shear. For Newtonian fluids the relation between the shear stress and the shear rate is linear and is given by $\tau = \eta\dot{\gamma}$, where η is the viscosity. However, most fluids do not show such behavior, meaning that η is a function of the shear rate, where as $\eta = \eta(\dot{\gamma})$, often called the shear viscosity. Fluids where the shear viscosity decreases with increasing shear rate are called shear-thinning fluids.

The shear viscosity displayed higher values depending on the magnetic field strength. The shear viscosities of MR fluids increased because more energy needed to break the chain-like or column structure assembled by the magnetic particles.[35]

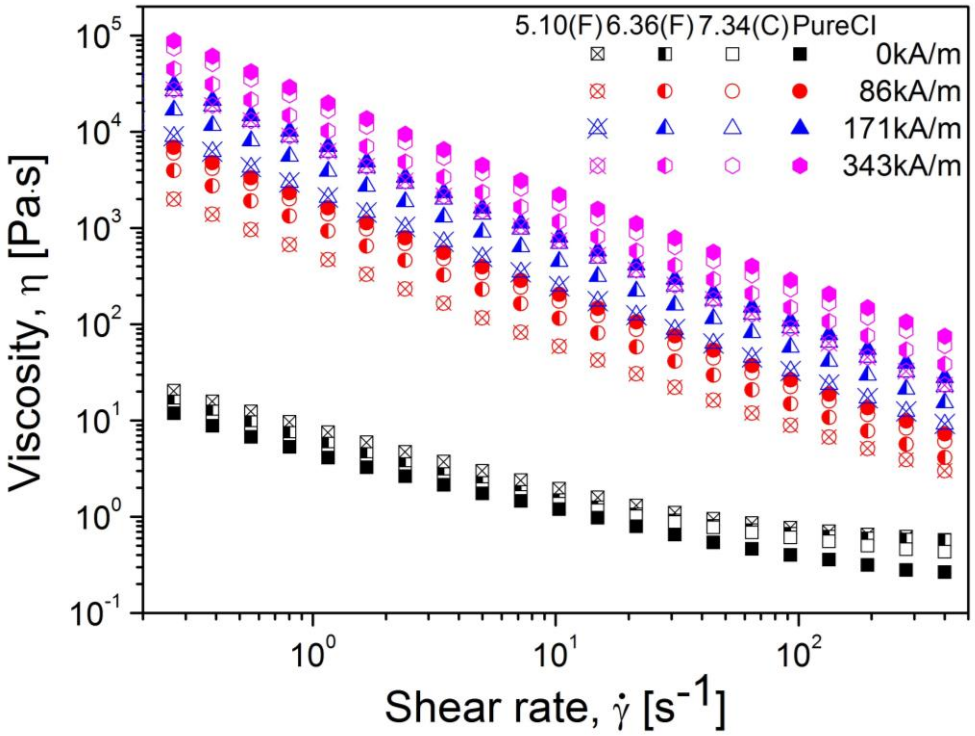

Figure 16. Shear viscosity flow curve for 20 vol% of pure CI, CI/PSC (7.34), CI/PSF (6.36), and CI/PSF (5.10) suspensions under different magnetic field strengths.

3.4.6 Steady Shear Flow Curve

The test was conducted with a constant shear rate at 1 rad s^{-1} in a certain period. It is clear, from Figure 17 that the shear stress and shear viscosity remain as constant under the steady shear rate of 1 rad s^{-1} and their value increased with the increase of magnetic field strength. This is because under the stationary shear, the breakage and formation rate of the fluid were almost the same, no yield stress loss occurred. Besides, stronger magnetic field applied contributed to the formation of stronger particles chains thus, shear stress and shear viscosity increased following the intensity of magnetic field.

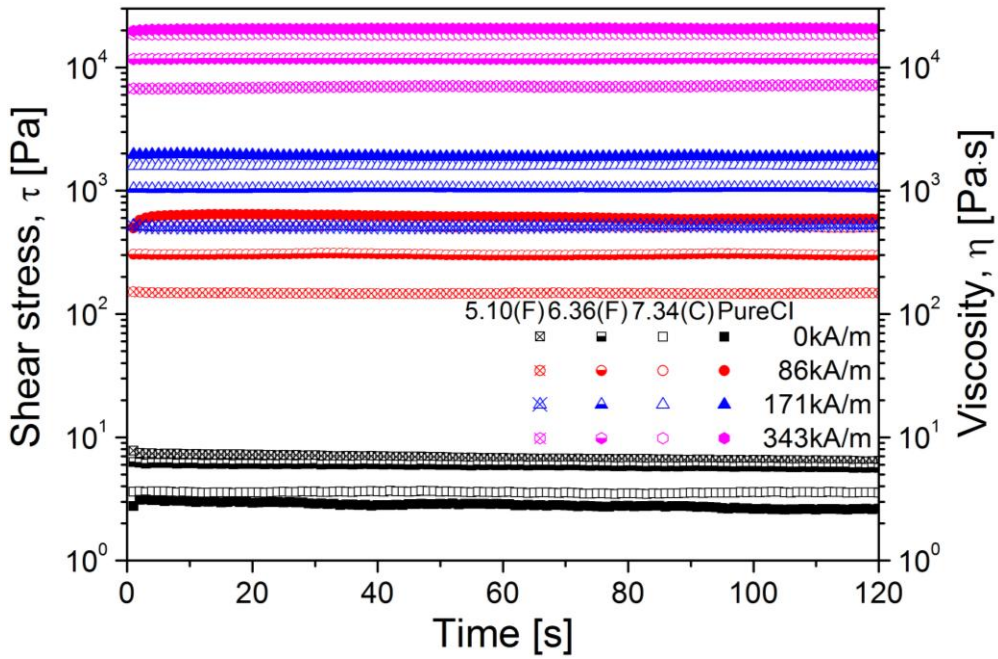

Figure 17. Shear stress and shear viscosity as a function of time for 20 vol% of pure CI, CI/PSC (7.34), CI/PSF (6.36), and CI/PSF (5.10) suspensions under different magnetic field strengths.

3.4.7 Static Yield Stress

The static yield stress was analyzed using the Controlled Shear Stress (CSS) mode which started the test in the rest state and increased the shear stress to a critical value at which the fluid began to flow. The shear viscosity was initially holding its value as a constant at the low shear stress region and subsequently at a certain high shear stress point, the value of shear viscosity plummeted abruptly in several orders of magnitude. This phenomena can be depicted and elucidated in microscopic level. As previously discussed, the magnetic particles forms chain-like structures when subjected to a magnetic field and the MR fluid becomes a viscoelastic solid with an extraordinary high viscosity because these chain-like structures hinder the flow of the fluid. A certain amount of shear stress has to be applied to break the chain-like structure assembled in the fluid in order to initiate the flow, so that the fluid can appear as a viscous liquid. In the current test, the viscosity of each MR fluid was measured by gradually increasing the shear stress exerted to the fluids. So, at a certain high shear stress point, the shear stress applied to the fluid was strong enough to break those chain-like structures, initiating the flow. In other words, the shear stress applied exceeded the yield stress that is required to begin the flow. Figure 18 shows the change in the viscosity as a function of the shear stress. From the points marked with the arrow, all of the curves show a fairly

sharp decrease in the shear viscosity. Therefore, the value of these points can be considered to be the static yield stress. The result revealed that pure CI had the highest static yield stress, following by the CI/PSC and then CI/PSF suspensions. The tendency of decreasing in yield stresses after coating and foaming modification in this study reaffirmed similar results obtained in shear stress flow curve and shear viscosity flow curve. The values of the static yield stress are summarized in Table 5.

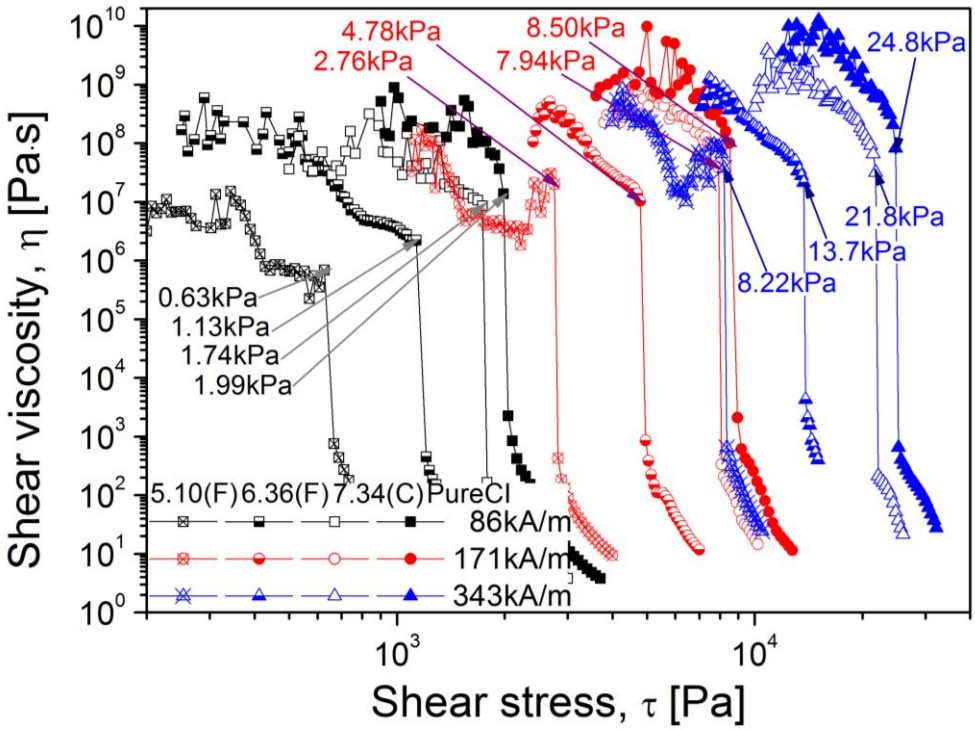

Figure 18. Static yield stress curve (CSS mode) for 20 vol% of pure CI, CI/PSC (7.34), CI/PSF (6.36), and CI/PSF (5.10) suspensions under different magnetic field strengths.

3.4.8 Dynamic Yield Stress Dependence on Applied Magnetic Field Strength

On the other hand, the yield stress dependence on the applied magnetic field strength was identified and the result is shown in Figure 19. The range of dynamic yield stress (taken from shear stress flow curve, summarized in Table 4) was divided into 2 regions.[39] Under a weak applied magnetic field, dynamic yield stress increases quadratic with increasing magnetic field strength, $\tau_{dy} \propto H^2$, while the magnetic field is increased, dynamic yield stress follows $\tau_{dy} \propto H^{1.5}$ at intermediate range of magnetic field strength. At low magnetic field strength, the dynamic yield stress is quadratically proportional to magnetic field intensity, H^2 due to the local saturation of the magnetized particles (Optimum magnetization).[40]

The magnetic polarization model was used in the present study to predict the relation between the field-dependent dynamic yield stress and the intensity of magnetic field applied.[22] Upon the application of magnetic field, the polarization force between the magnetic particles causes them to mutually attract and subsequently form chain-like structures. While at a sufficiently high magnetic field, the magnetization saturation occurs, and the polarization force fails to increase with increasing magnetic field intensity. Consequently,

the exponent declines from 2.0 (Optimum magnetization) to 1.5 due to the magnetization saturation of the magnetic particles.

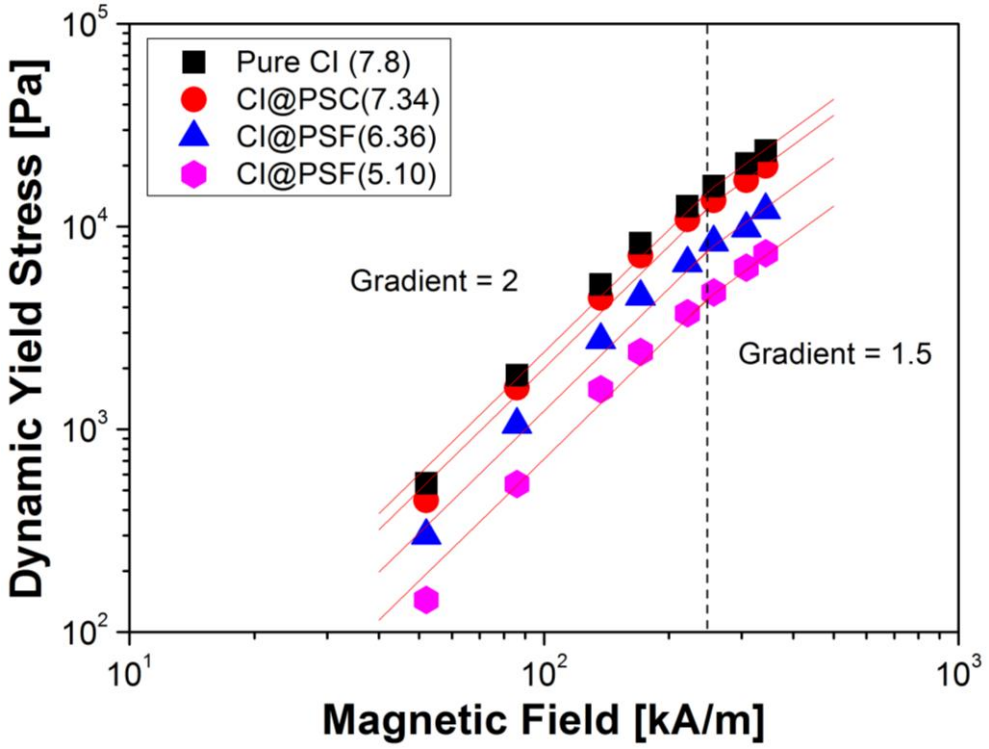

Figure 19. Dynamic yield stress dependence on the applied magnetic field strength for pure CI, CI/PSC (7.34), CI/PSF (6.36), and CI/PSF (5.10) suspensions.

Table 4. Dynamic yield stress for MR suspension based on each sample as a function of magnetic field strength.

Magnetic Field Strength [kA/m]	**Dynamic Yield Stress [Pa]**			
	Pure CI	CI/PSC (7.34)	CI/PSF (6.36)	CI/PSF (5.10)
86	1850	1608	1058	537
171	8264	7184	4516	2411
257	15840	13480	8370	4727
343	23680	19910	12070	7373

Table 5. Static yield stress for MR suspension based on each sample as a function of magnetic field strength.

Magnetic Field Strength [kA/m]	**Static Yield Stress [Pa]**			
	Pure CI	CI/PSC (7.34)	CI/PSF (6.36)	CI/PSF (5.10)
86	1989	1737	1134	626
171	8504	7936	4782	2757
257	16230	14290	9211	5187
343	24750	21760	13703	8215

There are two yield stresses for MR fluids, which are the dynamic yield stress, τ_{dy}, corresponds to the stress of the MR fluid that is completely broken down under continuous shearing, and the static (or frictional) yield stress, τ_{sy}, is the minimum stress required to cause the suspension to flow. The dynamic yield stress, τ_{dy} is an extrapolated value from the plateau region in a plot (in log-scale) of the shear stress as a function to shear rate (plot of shear stress flow curve). Meanwhile, the static yield stress is defined as the minimum shear stress required to induce continuous shear flow in an initially static sample (CSS mode). The two values are usually not equal. And in the current study, the dynamic yield stress is lower than the static yield stress, which they have a good agreement with theory.[3,37]

3.5 Sedimentation Stability.

The sedimentation properties for each sample were analyzed using Turbiscan, an optical analyzer, which measures the dispersion state from light scattering and transmission data, and derives the migration velocity of dispersion over time. The particle dispersion was contained in a cylindrical glass cell and illumination beam scanned the sample cell from bottom to top periodically. The transmission profile varied with the cell height over time upon sedimentation of particles in the suspension. This complete analysis mode enables the detection of the migration phenomena, i.e. the sedimentation pattern of suspensions.

Figure 20 shows the sedimentation profile as a function of time for each sample. The profile indicates the percentage of light transmitted through the sample as a function of time. The X axis and Y axis in the graph represent the time and the variations in the light transmitted through the sample cell. No transmission denotes that there were many dispersed particles and incident light could not be transmitted due to a homogenous dispersion blocking the transmission of light through the fluid. Then, the transmission increased gradually over time as a result of settling. In short, low transmission value [%] corresponded to good sedimentation stability. The pure CI suspension

exhibited the highest sedimentation percentage with 80% of transmission, which consequently means that pure CI particles settled rapidly and seriously during the same time duration (24 hours). Upon the reduction in its density after coating, the CI/PSC (7.34) suspension presented a lower sedimentation percentage with 64% of transmission. More importantly, the CI/PSF (6.36) and (5.10) suspensions achieved low sedimentation percentages with only 44% and 32% of transmission, respectively. This revealed that both foaming particles with lower density demonstrated better sedimentation stability. This phenomenon can be explained by the reduced mismatch in density. According to the general law of sedimentation, the decrease in the density of particles causes a decrease in the density mismatch with the fluid, consequently leading to an improvement in the sedimentation stability. The equation for general law of sedimentation is derived as follows.[41]

$$\mathrm{V}(\phi, \mathrm{d}) = \frac{|\rho_P - \rho_c| \times g \times d^2}{18 \times v \times \rho_c} \cdot \frac{[1-\phi]}{[1 + \frac{4{,}6\phi}{(1-\phi)^3}]}$$

Where V represents particle migration velocity (m s^{-1}), ρ_p denotes particle density (kg m^{-3}), ρ_c indicates continuous phase density (kg m^{-3}), v designates cinematic viscosity of continuous phase, g is gravity constant (9.81 m s^{-2}), d stands for diameter of particle and ϕ represents volume fraction.

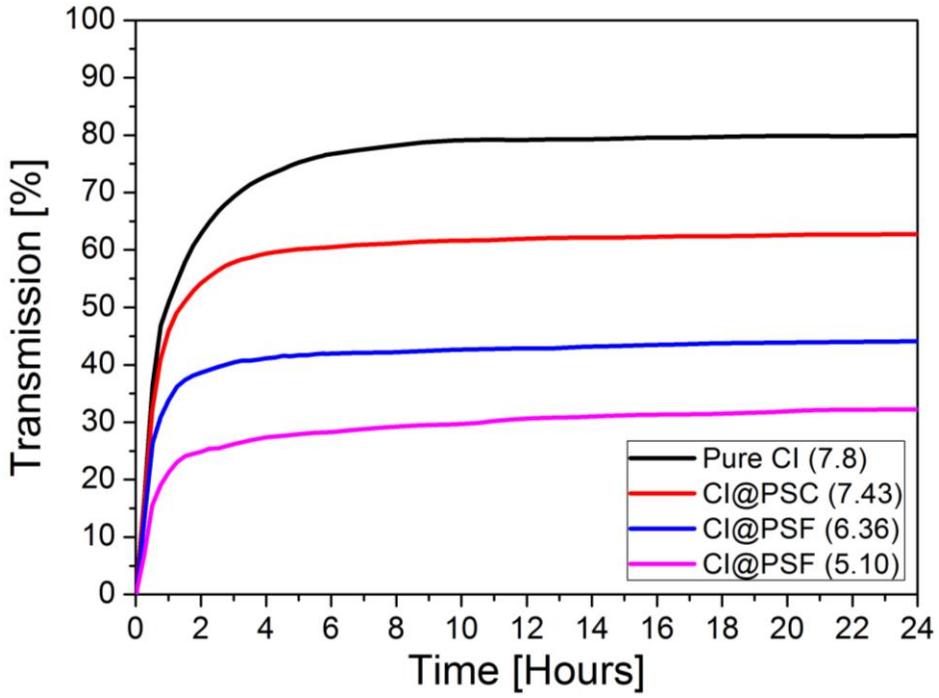

Figure 20. Change of transmission [%] as a function of time for (black) pure CI suspension, (red) CI/PSC (7.34), (blue) CI/PSF (6.36) and (magenta) CI/PSF (5.10).

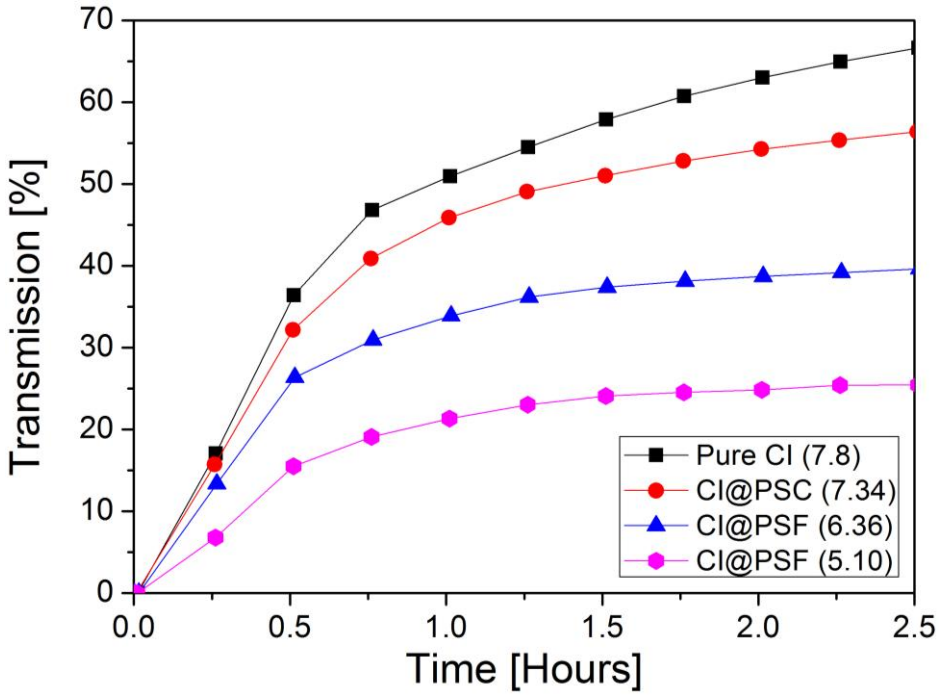

Figure 21. The magnified view of the sedimentation profile at an initial 2 hours.

Table 6. Density and particles migration velocity for Silicone Oil, Pure CI, CI/PSC (7.34), CI/PSF (6.36) and CI/PSF (5.10).

Samples	**Density [g cm^{-3}]**	**Particles Migration Velocity [mm min^{-1}]**
Silicone Oil (50cS)	0.96	—
Pure CI	7.80	0.0693
CI/PSC (7.34)	7.34	0.0677
CI/PSF (6.36)	6.36	0.0630
CI/PSF (5.10)	5.10	0.0560

Apparently, the dispersed particles in all four suspensions settled rapidly at the initial 2 hours and tend to get stable. Therefore, a magnified view of the sedimentation profile at the initial 2 hours was taken and depicted in Figure 21. A comparison in the sedimentation velocity of these four suspensions was carried out and the result was summarized in Table 6. The settling rate (particle migration velocity) for the initial 2 hours of each suspension was computed. The particle migration velocity (slope of the transmission as a functions of time) for pure C I suspension was the highest, following by CI/PSC (7.34), then CI/PSF (6.36), and lastly CI/PSF (5.10). The result unveiled that the particles migration velocity for the pure CI suspension was 0.0693 mm/min, the CI/PSC (7.34) suspension was 0.0677 mm/min, and the CI/PSF (6.36) and (5.10) suspension were 0.0630 mm/min and 0.0560 mm/min, respectively. It is obvious that the pure CI and CI/PSC (7.34) suspensions had a quite similar settling rate meanwhile the CI/PSF (6.36) and (5.10) suspensions demonstrated a slower settling profile. These results indicated that the CI/PSF (6.36) and (5.10) suspensions were more stable than the pure CI and CI/PSC (7.34) suspensions.

This stability was attributed to 3 primary factors, which are the reduction of mismatch in density, foaming particles produced a rough surface and PS organic surface improved the compatibility (the wettability and surface free

energy) with silicone oil. As aforementioned in the BET surface area analysis (refer to Table 3), it appears that the foaming particles had a higher specific surface. The rough surfaces delayed the settling because the increased surface area resulted in greater hydrostatic interactions and friction.[19] Besides, the PS organic surfaces may be refine the particle's wettability with silicone oil.[14] Furthermore, according to the general law of sedimentation, there are numerous factors which manipulate the sedimentation rate (i.e. particles migration velocity), including particle density, suspending fluid density, viscosity of suspending fluid, particle size, and finally volume fraction. To decrease the sedimentation rate, we may reduce the particle density and particle size, or increase the suspending fluid density and its viscosity, also adding the volume fraction of particles in the suspending fluid.

CHAPTER 4. CONCLUSION

As a conclusion, the present work attempted to reduce sedimentation in CI-based MR fluids by first coating a PS layer on the CI particles surfaces following by the foaming of the PS coating layer using the $scCO_2$ foaming processing to produce a core-shell structured CI coated with PS Foam (CI/PSF) particle. We have demonstrated an easy and reproducible way to prepare the CI/PSF particles. The incorporation of polymer foam with magnetic carbonyl iron particles results in a marked decrease in the particle density. As shown in the current studies, MR fluids utilizing CI coated with PS foam particles exhibit remarkable stability against sedimentation owing to the reduction of mismatch in density, foaming particles rough surface morphologies and PS organic surface improved the compatibility (the wettability and surface free energy) with silicone oil. However, a significant shortcoming of suspensions containing this kind of particles is that the maximum yield stress of the MR fluid is reduced associated with the decrease in particle density. The foaming produced particles displayed lower MR performances under an applied magnetic field because of the deterioration in their magnetization saturation. The enhancement of sedimentation stability makes MR fluids particularly suitable for civil engineering applications. For instance, earthquake protection system for skyscrapers. Due to the transient nature of seismic events, these

dampers never see regular motion, which can re-mix the fluid, therefore, they require high sedimentation stability. An optimization can be made by taking advantage of the improved sedimentation stability to a certain impressive level with a relevant controllable yield stresses.

CHAPTER 5. REFERENCES

1. Swan, J. W.; Vasquez, P. A.; Whitson, P. A.; Fincke, E. M.; Wakata, K.; Magnus, S. H.; De Winne, F.; Barratt, M. R.; Agui, J. H.; Green, R. D.; Hall, N. R.; Bohman, D. Y.; Bunnell, C. T.; Gast, A. P.; Furst, E. M., Multi-scale kinetics of a field-directed colloidal phase transition. *Proceedings of the National Academy of Sciences of the United States of America* **2012,** *109* (40), 16023-8.
2. Bica, I.; Liu, Y. D.; Choi, H. J., Physical characteristics of magnetorheological suspensions and their applications. *Journal of Industrial and Engineering Chemistry* **2013,** *19* (2), 394-406.
3. Seo, Y. P.; Choi, H. J.; Lee, J. R.; Seo, Y., Modeling and analysis of an electrorheological flow behavior containing semiconducting graphene oxide/polyaniline composite particles. *Colloids and Surfaces A: Physicochemical and Engineering Aspects* **2014,** *457*, 363-367.
4. Liu, Y. D.; Lee, J.; Choi, S. B.; Choi, H. J., Silica-coated carbonyl iron microsphere based magnetorheological fluid and its damping force characteristics. *Smart Materials and Structures* **2013,** *22* (6), 065022.
5. ACHEN, A.; TOSCANO, J.; MARJORAM, R.; StCLAIR, K.; McMAHON, B.; GOELZ, A.; SHUTTO, S.; France, L. In *Semi-active vehicle cab suspension using magnetorheological (MR) technology*, Symposium on Fluid Power, 2008.
6. Park, B. J.; Fang, F. F.; Choi, H. J., Magnetorheology: materials and application. *Soft Matter* **2010,** *6* (21), 5246.
7. Phule, P. P., Magnetorheological (MR) fluids: principles and applications. *Smart Materials Bulletin* **2001,** *2001* (2), 7-10.
8. Carlson, J. D.; Jolly, M. R., MR fluid, foam and elastomer devices. *mechatronics* **2000,** *10* (4), 555-569.
9. Chen, Z.; Wang, X.; Ko, J.; Ni, Y.; Spencer Jr, B. F.; Yang, G. In *MR damping system on Dongting Lake cable-stayed bridge*, Smart Structures and Materials, International Society for Optics and Photonics: 2003; pp 229-235.
10. Bitaraf, M.; Ozbulut, O. E.; Hurlebaus, S.; Barroso, L., Application of semi-active control strategies for seismic protection of buildings with MR dampers. *Engineering Structures* **2010,** *32* (10), 3040-3047.
11. Jain, V. K.; Sidpara, A.; Sankar, M. R.; Das, M., Nano-finishing techniques: a review. *Proceedings of the Institution of Mechanical Engineers, Part C: Journal of Mechanical Engineering Science* **2011,** *226* (2), 327-346.

12. Quan, X.; Chuah, W.; Seo, Y.; Choi, H. J., Core-Shell Structured Polystyrene Coated Carbonyl Iron Microspheres and their Magnetorheology. *Magnetics, IEEE Transactions on* **2014,** *50* (1), 1-4.
13. Cho, M. S.; Lim, S. T.; Jang, I. B.; Choi, H. J.; Jhon, M. S., Encapsulation of spherical iron-particle with PMMA and its magnetorheological particles. *Magnetics, IEEE Transactions on* **2004,** *40* (4), 3036-3038.
14. Sedlacik, M.; Pavlinek, V., A tensiometric study of magnetorheological suspensions' stability. *RSC Adv.* **2014,** *4* (102), 58377-58385.
15. Jolly, M. R.; Bender, J. W.; Carlson, J. D., Properties and applications of commercial magnetorheological fluids. *Journal of Intelligent Material Systems and Structures* **1999,** *10* (1), 5-13.
16. Shah, K.; Phu, D. X.; Seong, M.-S.; Upadhyay, R. V.; Choi, S.-B., A low sedimentation magnetorheological fluid based on plate-like iron particles, and verification using a damper test. *Smart Materials and Structures* **2014,** *23* (2), 027001.
17. López-López, M.; De Vicente, J.; Bossis, G.; González-Caballero, F.; Durán, J., Preparation of stable magnetorheological fluids based on extremely bimodal iron–magnetite suspensions. *Journal of materials research* **2005,** *20* (04), 874-881.
18. Pramudya, I.; Sutrisno, J.; Fuchs, A.; Kavlicoglu, B.; Sahin, H.; Gordaninejad, F., Compressible Magnetorheological Fluids Based on Composite Polyurethane Microspheres. *Macromolecular Materials and Engineering* **2013,** *298* (8), 888-895.
19. BELL, R.; ZIMMERMAN, D.; WERELEY, N., Magnetorheology of Fe Nanofibers Dispersed in a Carrier Fluid. *Magnetorheology: Advances and Applications* **2013,** *6*, 31.
20. LIU, Y. D.; CHOI, H. J., Coated Magnetorheological Composite Particles: Fabrication and Rheology. *Magnetorheology: Advances and Applications* **2013,** *6*, 156.
21. Chiriac, H.; Stoian, G., Influence of the particles size and size distribution on the magnetorheological fluids properties. *Magnetics, IEEE Transactions on* **2009,** *45* (10), 4049-4051.
22. Fang, F. F.; Liu, Y. D.; Choi, H. J.; Seo, Y., Core-shell structured carbonyl iron microspheres prepared via dual-step functionality coatings and their magnetorheological response. *ACS applied materials & interfaces* **2011,** *3* (9), 3487-95.

23. Fang, F. F.; Choi, H. J.; Seo, Y., Sequential coating of magnetic carbonyliron particles with polystyrene and multiwalled carbon nanotubes and its effect on their magnetorheology. *ACS applied materials & interfaces* **2010,** *2* (1), 54-60.
24. Strauss, W.; D'Souza, N. A., Supercritical CO2 processed polystyrene nanocomposite foams. *Journal of cellular plastics* **2004,** *40* (3), 229-241.
25. Reverchon, E.; Cardea, S., Production of controlled polymeric foams by supercritical CO2. *The Journal of Supercritical Fluids* **2007,** *40* (1), 144-152.
26. Liao, X.; Zhang, H.; He, T., Preparation of Porous Biodegradable Polymer and Its Nanocomposites by Supercritical CO2Foaming for Tissue Engineering. *Journal of Nanomaterials* **2012,** *2012*, 1-12.
27. Leitner, W., Green chemistry: designed to dissolve. *Nature* **2000,** *405* (6783), 129-130.
28. Huang, S.; Wu, G.; Chen, S., Preparation of open cellular PMMA microspheres by supercritical carbon dioxide foaming. *The Journal of Supercritical Fluids* **2007,** *40* (2), 323-329.
29. Hinokawa, A.; Shioya, S.; Tokoro, H., Production method of foamed particles of polyolefin resin. Google Patents: 1994.
30. Alessi, P.; Cortesi, A.; Kikic, I.; Vecchione, F., Plasticization of polymers with supercritical carbon dioxide: Experimental determination of glass-transition temperatures. *Journal of Applied Polymer Science* **2003,** *88* (9), 2189-2193.
31. Mrlik, M.; Ilcikova, M.; Pavlinek, V.; Mosnacek, J.; Peer, P.; Filip, P., Improved thermooxidation and sedimentation stability of covalently-coated carbonyl iron particles with cholesteryl groups and their influence on magnetorheology. *Journal of colloid and interface science* **2013,** *396*, 146-51.
32. Kim, Y. J.; Liu, Y. D.; Seo, Y.; Choi, H. J., Pickering-emulsion-polymerized polystyrene/Fe2O3 composite particles and their magnetoresponsive characteristics. *Langmuir : the ACS journal of surfaces and colloids* **2013,** *29* (16), 4959-65.
33. Upadhyay, R.; Laherisheth, Z.; Shah, K., Rheological properties of soft magnetic flake shaped iron particle based magnetorheological fluid in dynamic mode. *Smart Materials and Structures* **2014,** *23* (1), 015002.
34. Mrlik, M.; Sedlacik, M.; Pavlinek, V.; Bazant, P.; Saha, P.; Peer, P.; Filip, P., Synthesis and magnetorheological characteristics of ribbon-like, polypyrrole-coated carbonyl iron suspensions under oscillatory shear. *Journal of Applied Polymer Science* **2013,** *128* (5), 2977-2982.

35. Kim, J. E.; Choi, H. J., Magnetic carbonyl iron particle dispersed in viscoelastic fluid and its magnetorheological property. *Magnetics, IEEE Transactions on* **2011,** *47* (10), 3173-3176.
36. Mehdizadeh, A.; Mei, R.; Klausner, J. F.; Rahmatian, N., Interaction forces between soft magnetic particles in uniform and non-uniform magnetic fields. *Acta Mechanica Sinica* **2010,** *26* (6), 921-929.
37. Seo, Y. P.; Seo, Y., Modeling and analysis of electrorheological suspensions in shear flow. *Langmuir : the ACS journal of surfaces and colloids* **2012,** *28* (6), 3077-84.
38. Andablo-Reyes, E.; Hidalgo-Á lvarez, R.; de Vicente, J., Controlling friction using magnetic nanofluids. *Soft Matter* **2011,** *7* (3), 880.
39. Fang, F. F.; Choi, H. J.; Jhon, M. S., Magnetorheology of soft magnetic carbonyl iron suspension with single-walled carbon nanotube additive and its yield stress scaling function. *Colloids and Surfaces A: Physicochemical and Engineering Aspects* **2009,** *351* (1), 46-51.
40. Zhang, W. L.; Liu, Y. D.; Choi, H. J., Field-responsive smart composite particle suspension: materials and rheology. *Korea-Australia Rheology Journal* **2012,** *24* (3), 147-153.
41. Mills, P.; Snabre, P., Settling of a suspension of hard spheres. *EPL (Europhysics Letters)* **1994,** *25* (9), 651.

요약 (국문초록)

자기유변유체는 물 또는 비수계(실리콘 오일 등)의 유체에 자화 가능한 미세입자(철 마이크로 입자)를 분산시킨 현탁액으로서, 외부로부터 제공되는 강한 자기장에 따라 탄성, 소성, 점도 같은 자기유변효과를 나타내는 유체를 말한다. 자기유변유체는 외부 자기장에 의해 유변효과를 조절할 수 있기 때문에 다양한 응용분야로의 적용 가능성에 대한 관심이 증가하고 있다. 그러나 자성입자(철 마이크로 입자)와 현탁 유체와의 밀도 차에 의해 발생하는 침전현상으로 인해 자기유변유체의 실제적인 응용이 제한되고 있다. 특히 기존에 널리 사용되는 카르보닐 철 마이크로 입자는 강한 자화성과 적당한 크기 (1-10μm)를 가지고 있지만 상대적으로 무거운 특성 때문에 침전문제가 현저하다고 알려져 있다.

본 연구에서는 이러한 자기유변유체의 침전현상을 개선하기 위해 특별한 이중처리공정을 도입하여 마이크로 입자를 제조하였다. 사용된 이중처리공정은 1) 카르보닐 철 마이크로 입자의 표면에 폴리스티렌 고분자를 코팅하여 코어-쉘 구조의 카르보닐 철-폴리스티렌 복합재료를 만드는 코팅과정과 2) 초임계 이산화탄소 유체를

이용해 코팅된 폴리스티렌 고분자 쉘을 발포하는 발포과정으로 구성된다.

이렇게 제조된 마이크로 입자의 특성 및 마이크로 입자를 이용한 자기유변유체의 자기유변학적 특성을 다양한 분석 방법을 통해 측정하였다. 피크노미터 결과, 코팅 이후 약 5% 그리고 발포 이후 35%의 밀도 감소를 확인하였고, 전자현미경 (SEM)과 BET 비표면적측정기 측정을 통해 코팅과 발포공정이 성공적으로 진행되었음을 확인하였다. 그리고 회전형 레오미터를 사용하여 측정한 자기유변유체의 다양한 자기유변학적 특성에서는 새로운 마이크로 입자의 밀도, 표면 특성이 초래하는 자기유변유체의 유변학적 성질의 변화를 확인하였다. 마지막으로 터비스캔 장치를 이용하여 측정된 침전특성 분석에서 기존의 마이크로 입자 대비 향상된 침전특성을 보이는 것을 확인하였다.

결론적으로, 이중 처리공정을 통해 새롭게 제조된 낮은 밀도를 갖는 마이크로 입자를 이용한 자기유변유체는 물성 및 표면 특성 때문에 기존에 사용되던 자기유변유체 대비 우수한 침전속도, 침전안정성을 보여주었으며, 이는 코팅과 발포로 구성된 이중처리공

정이 자기유변유체의 침전문제를 개선하기 위한 새롭고 효율적인 방법임을 본 연구를 통해 확인하였다.

주요어 : **자기유변유체, 카르보닐 철, 발포 폴리스티렌 폼, 코어-쉘 구조, 초임계 이산화탄소 유체.**

학 번 : 2013-22470